AD-759 507

MELT-GROWN OXIDE-METAL COMPOSITES

Alan T. Chapman, et al

Georgia Institute of Technology

Prepared for:

Advanced Research Projects Agency

January 1973

REPORT NO. 5

MELT-GROWN OXIDE-METAL COMPOSITES

SEMI-ANNUAL TECHNICAL REPORT

(Period: 10 June 1972 to 9 December 1972)

Project Director
A. T. Chapman

Principal Investigators
J. F. Benzel J. K. Cochran
R. K. Feeney F. W. Ling
J. D. Norgard

Sponsored By
Advanced Research Projects Agency
Department of Defense

ARPA ORDER NO. 1637

Contract No. DAAH01-71-C-1046

January 1973

1973

School of Ceramic Engineering
GEORGIA INSTITUTE OF TECHNOLOGY
Atlanta, Georgia

Unclassified

Security Classification

DOCUMENT CONTROL DATA - R & D

Security classification of title, body of abstract and indexing annotation must be entered when the overall report is classified

1 ORIGINATING ACTIVITY (Corporate author)

School of Ceramic Engineering
Georgia Institute of Technology

2a. REPORT SECURITY CLASSIFICATION

Unclassified

2b GROUP

3 REPORT TITLE

MELT-GROWN OXIDE-METAL COMPOSITES

4 DESCRIPTIVE NOTES (Type of report and inclusive dates)

Semi-Annual (10 June 1972 - 9 December 1972)

5 AUTHOR(S) (First name, middle initial, last name)

Alan T. Chapman, James F. Benzel, J. K. Cochran, Robert K. Feeney, F. W. Long, J. D. Norgard

6 REPORT DATE

January 1973

7a. TOTAL NO OF PAGES

~~102~~ 43

7b. NO. OF REFS

9

8a CONTRACT OR GRANT NO.

DAAH01-71-C-1046

b PROJECT NO

9a. ORIGINATOR'S REPORT NUMBER(S)

E18-604-5

c

9b. OTHER REPORT NO(S) (Any other numbers that may be assigned this report)

ARPA ORDER NO. 1637

d

10 DISTRIBUTION STATEMENT

Distribution of this document is unlimited.

11 SUPPLEMENTARY NOTES

12. SPONSORING MILITARY ACTIVITY

Advanced Research Projects Agency
1400 Wilson Boulevard
Arlington, Virginia 22209

13 ABSTRACT

This research is designed to develop melt-grown oxide-metal composite structures for high field electron emission testing. A number of refractory oxide-metal mixtures (i.e. UO_2-W, stabilized ZrO_2 and HfO_2-W, UO_2-Ta, and the rare earth oxides of Gd_2O_3, Nd_2O_3 and La_2O_3-Mo and W) have been successfully induction melted and unidirectionally solidified to form aligned metallic fibers embedded in the oxide matrix. The system CeO_2-Mo was added to this list this report period. The chemical etching behavior of UO_2-W and CeO_2 doped Gd_2O_3-Mo samples was extensively studied to establish conditions for forming a variety of desirable emitter configurations. Experimental electron emission testing has progressed through the use of better samples and improved etching and brazing procedures to the point where bulk emission currents of several hundred mA/cm^2 can be routinely obtained. One emission sample yielded over 0.5 A/cm^2 for several hours, with no apparent damage to the emitter pins, before the diode assembly failed and terminated the experiment. A three-dimensional numerical approxiamtion is being used to theoretically analyze the field emission performance of various pin array geometries.

DD FORM NOV 65 1473 (PAGE 1)

S/N 0101 07.6801

Unclassified

Security Classification

14. KEY WORDS	LINK A		LINK B		LINK C	
	ROLE	WT	ROLE	WT	ROLE	WT
Oxide-Metal Composites		4				
Field Emission		4				
Rf Heating		3				
Field Emission Theory		3				
Oxides		2				
Refractory Metals		2				
Unidirectional Solidification		4				
Eutectic Structures		3				
UO_2		2				
ZrO_2 (Stabilized)		1				
HfO_2 (Stabilized)		1				
Gd_2O_3		2				
Nd_2O_3		2				
La_2O_3		2				
CeO_2		2				
Internal Melting		3				
Etching		2				
Tungsten Fibers		4				
Molybdenum Fibers		4				
Electron Emitting Arrays		4				
Oxide-Metal Solidification		3				
High Field Emission		4				

ja

DD FORM 1 NOV 1473 (BACK)
S/N 0102-014-6800

PERSONNEL PARTICIPATING IN PROJECT

Principal Investigators	Graduate Students
J. F. Benzel	Marshall Burke
J. K. Cochran	J. A. Graves
R. K. Feeney	B. A. Keener
F. W. Ling	W. L. Ohlinger
J. D. Norgard	M. C. Pao
	A. V. Petty
	G. B. Ricks
	J. W. Stendera
	J. O. Tarter
	M. D. Watson

TABLE OF CONTENTS

LIST OF ILLUSTRATIONS

LIST OF ILLUSTRATIONS (Continued)

LIST OF ILLUSTRATIONS (Continued)

LIST OF ILLUSTRATIONS (Continued)

LIST OF TABLES

FOREWARD

This research was supported by the Advanced Research Projects Agency of the Department of Defense and was monitored by the U. S. Army Missile Command under Contract Number DAAH01-71-C-1046.

"The views and conclusions contained in this document are those of the authors and should not be interpreted as necessarily representing the official policies, either expressed or implied, of the Advanced Research Projects Agency or the U. S. Government."

SECTION I

INTRODUCTION

This is the fifth report describing research performed on the "Melt-Grown Oxide-Metal Composites" Project, ARPA Order Number 1637, and also the Semi-Annual Technical Report for Contract DAAH01-71-C-1046, covering the report period of June 10, 1971 through December 9, 1972. The information contained in this Report will emphasize work accomplished since the Annual Report[1], although some of the earlier information will be repeated to provide informational continuity. Previous reports[1,2,3,4] contained a detailed description of the modified floating zone technique employed during the growth of the oxide-metal composite structures containing many millions of less than 1 micron diameter metallic fibers per cm^2 uniformly embedded in an oxide (insulating or semi-conducting) matrix, and this information will not be covered in this Report.

The primary technical objective of this study is to understand the growth processes leading to coupled growth and ordered microstructures during the controlled solidification of refractory oxide-metal mixtures, and to successfully produce useable samples of these composites and evaluate their potential for electronic applications, with the primary

emphasis on electron field emission. The research program is divided into five areas, and the objectives of these project areas and the work underway in each is briefly outlined in this Section.

A. SOLIDIFICATION BEHAVIOR OF OXIDE-METAL MIXTURES

A study of the chemical, thermal, electrical and mechanical variables active during the solidification of numerous oxide-metal mixtures is in progress to interpret and understand the parameters that control the successful growth of oxide-metal composites. Of fundamental importance are the factors which impart and control the metal solubility in the molten oxides. Oxides which possess variable stoichiometry appear to dissolve the refractory metals more effectively than the compounds of fixed stoichiometry. Analysis of microstructural data in a variety of systems has indicated some interesting variations in metal content (eutectic composition) with composite growth rate. The initial electron beam melting of oxide-metal mixtures contained in crucibles is reported.

B. FORMATION OF OPTIMUM EMITTING ARRAYS

Selective chemical etching studies to expose, shape and remove the metallic pins from the oxide-metal composites to obtain structures of interest for emission testing have

continued. A series of detailed etching studies were performed on UO_2-W samples to find conditions which yield reproducible structures. The initial work to expose and point Mo pins in CeO_2 doped Gd_2O_3-Mo samples are reported.

C. OXIDE-METAL COMPOSITE PROPERTIES

Work in this area is designed to explore any and all properties of these materials which are unique and potentially useful for practical applications. The property measurements were interrupted this report period as the major effort was spent developing suitable brazing materials and procedures for use with the composite samples. Adequate brazing is required before additional electrical measurements can be undertaken.

D. EXPERIMENTAL EMISSION MEASUREMENTS

The electron emission performance of oxide-metal composites is being evaluated as a function of pin array geometry and such electrical variables as field strength and interelectrode spacing. Emission measurements are conducted under carefully controlled conditions so that the onset of physical damage to the emitter structure can be determined.

Two new diode assemblies, one with fixed interelectrode spacing and a large heat dissipation capability and the other a demountable assembly for long-term emission testing, were

constructed and tested. Improved composite structures, brazing and conditioning procedures have produced samples with bulk current densities of 0.5 A/cm^2. Increased experience testing these materials as field effect emitters has lead to proposed procedures for preconditioning the pins for improved current sharing behavior. The conditions favoring electrical breakdown across the test diode are also considered. The initial pulsed mode emission data are reported.

E. THEORETICAL ANALYSIS OF ELECTRON EMITTING ARRAYS

In the previous work, a two-dimensional analysis of the effects of different array geometries on the total emission current from an electron emitting array was considered. In the present study, the actual three-dimensional case is being analyzed using a numerical approximation. The work has progressed to the extent that the emission current from an array of limited size can be determined.

SECTION II

SOLIDIFICATION BEHAVIOR OF OXIDE-METAL MIXTURES

This section is subdivided into four major subsections: A) Induction Coupling and Solidification Behavior of Oxide-Metal Systems, B) Variation of Eutectic Compositions with Growth Rate, C) Electron Beam Melting and Solidification of Oxide-Metal Systems, and D) X-ray Analysis of Oxide-Metal Composites. These subsections cover investigations designed to develop new oxide-metal systems that are capable of being internally melted by high frequency induction heating, development of techniques designed to grow oxide-metal composites suitable for high field electron emission testing, the determination of some of the parameters which control the successful growth of oxide-metal composites, and the initiation of research into the use of an electron-beam zone refiner to investigate oxide-metal systems that cannot be internally melted by direct induction heating.

A. INDUCTION COUPLING AND SOLIDIFICATION BEHAVIOR OF OXIDE-METAL MIXTURES

Melting and subsequent controlled solidification of refractory oxides and oxide-metal mixtures have been previously reported[1-4] using high (4 to 30 MHz) frequency rf heating. This technique is limited to systems that have sufficient electrical conductivity at elevated temperatures

to support eddy current heating at the level required to produce internal melting.

During this report period a number of major accomplishments have been achieved in the ordered growth of metal fibers in oxide matrices. These include: 1) extensive ordered growth in the Gd_2O_3-CeO_2-Mo system and the fabrication of composite rods in this system up to 5 cm long; 2) the development of growth parameters designed to achieve "steady state" conditions during solidification in the UO_2-W system; 3) the initial ordered oxide-metal composite growth in the CeO_2-Mo system; 4) the calculation of the eutectic composition of the Y_2O_3 stabilized HfO_2-W system, and determination that the eutectic composition for several of the oxide-metal systems varies with growth rate; and 5) the successful induction melting of two Al_2O_3-based systems.

This subsection is subdivided into four areas based on the oxide matrix materials.

1. Stabilized ZrO_2-W and HfO_2-W
2. UO_2-W
3. Rare Earth Oxide-Metal
4. (Al_2O_3-Cr_2O_3)-W or Mo

1. Yttria Stabilized ZrO_2-W and HfO_2-W

In the last report[1] a detailed description of the influence of rf frequency, Y_2O_3 and W content, and growth rate on composite growth in Y_2O_3 stabilized ZrO_2-W samples was described. Some further work was performed to assess the influence of atmosphere on growth in this system. Previously reported[1]

were growth experiments in which ZrO_2 + 10 mole % Y_2O_3 and 8 and 16 weight % W were melted in a H_2 atmosphere. These samples displayed oxide-metal composite growth throughout the entire solidified area (without the areas of primary oxide normally seen in the upper portion of the samples solidified in N_2-H_2 mixtures); however, extensive regions of W dendrites were also formed.

A series of ZrO_2 + 10 mole % Y_2O_3 experiments with W contents less than 8 w/o were run to find the optimum W addition for samples melted in H_2. Samples grown with about 6.5 w/o W virtually eliminated the formation of W dendrites and contained fibers throughout the entire solidified area, but were interrupted occasionally by bands of pure oxide or areas of oxide containing non-uniform W platelets or needles. Calculation of the W content before and after growth in those samples solidified in H_2 indicated that very little W was lost from the rods by vaporization during growth. Samples previously solidified in N_2-H_2 mixtures which initially contained 16 w/o W lost so much W by vaporization that the good growth areas contained only about 6 w/o W and the upper portions of the rod, which typically contained primary oxide areas, retained even less W.

Only limited study of the ZrO_2-W system is anticipated in the future, primarily because the other oxide-metal systems can be readily etched to form ideal emitting arrays, and the successful growth of ZrO_2-W composites is a critical operation sensitive to a great many minor growth variations.

An analysis of well ordered eutectic areas in a previously grown Y_2O_3 stabilized HfO_2-W sample was made to estimate the eutectic composition in this system. The sample composed of HfO_2 with 10 m/o Y_2O_3 and initially 12.3 w/o W was found to contain only 2.5 w/o W in the final eutectic structure. This is a reasonable eutectic composition for Y_2O_3 stabilized HfO_2 and W. This composition was determined by measuring fiber diameters and counting fiber densities on SEM micrographs and then using 9.75 and 19.27 gm/cm^3 as the theoretical densities of HfO_2 stabilized with 10 m/o Y_2O_3[5] and tungsten respectively to convert from volume percent to weight percent tungsten. The tungsten content in the molten zone apparently decreased throughout the growth process by vaporization of W, WO_2 and WO_3 which were detected in vapor coatings deposited on the quartz atmosphere containment tube. No future work is planned in the HfO_2-W area, primarily because of the severe cracking problems.

2. UO_2-W

In previous reports,[1,2] the importance of the O/U ratio on composite growth in the system UO_2-W was reviewed. The influence of the O/U ratio on the sintering and rf coupling characteristics of the UO_2-W samples and on the melting and solidification kinetics of composite structures were described in detail. Special emphasis was placed on the influence of the O/U ratio on the solubility of tungsten in molten UO_2. During the present report period, work in this system was

designed to select growth conditions which would yield reproducible structures containing ordered arrays of continuous W fibers and provide samples suitable for slicing numerous wafers from the same rod for the fabrication of emission test samples.

Initial experiments employed minor modifications of the typical growth conditions used previously, i.e. mixtures of $UO_{2.14}$ plus 10 w/o W were induction melted in N_2-H_2 atmospheres, and molybdenum pre- and post-heaters were utilized. Generally these conditions produced an area of good composite growth near the base of the sample; however, the upper portions of the solidified sample routinely displayed the oxide-rich banded-type structure and areas of limited W solubility.

Work in the UO_2-W system was next modified to find an intermediate oxygen potential using CO/CO_2 atmospheres which would provide sufficient tungsten solubility to produce cells that run the entire length of the molten zones. The runs were performed using various mixtures of N_2 and a premixed gas tank containing 10^4 ppm CO_2 in CO. The atmosphere was varied between 80% N_2- 20% CO_2/CO to 100% CO_2/CO. The samples were prepared by mixing $UO_{2.14}$ powder with 10 w/o W and induction melting using the standard method. The results are summarized in Table I. Although some fair composite growth was achieved, the results were not a significant improvement over samples grown in N_2-H_2 atmospheres.

TABLE I

SUMMATION OF EUTECTIC GROWTH RESULTS USING $UO_{2.14}$ +10w/o W SAMPLES IN N_2-CO_2/CO ATMOSPHERES

Experiment Number	Growth Atmosphere % CO_2/CO*	% N_2	Growth Rate cm/hr.	Comments
27-4	20	80	2.40	Long cell growth with banding. Good overall fiber growth.
27-5	50	50	2.18	Good cell growth. Banding.
27-7	80	20	1.96	Insufficient melt formed for composite growth.
27-8	80	20	2.52	Numerous long cells, large number of short cells. Banding.
27-9	-	100	2.85	Some long cells. Many short cells. Banding.
27-10	100	-	2.30	Long cells, good fiber growth in top and bottom. Banding.

* Pre-Mixed Tank Containing 10^4 ppm CO_2 in CO.

The latest efforts to grow reproducible UO_2-W samples suitable for fabrication of emission test samples has centered around achieving "steady state" growth conditions. In this approach the entire length of the interior of the UO_2-W rod was melted with the intent of maintaining a constant temperature and a uniform concentration of W dissolved in the molten oxide. To achieve these conditions the whole rod was exposed to the rf field (by removing the molybdenum pre- and post-heaters from the rf coil), and the unmelted skin acted as a crucible to contain a two to three centimeter long molten zone. The sample was lowered in an oxygen partial pressure maintained with CO/CO_2 mixtures designed to keep the stoichiometry of the melt above 2.00. Using this technique, it was possible to start with the low O/U ratio powder (2.04) and obtain good composite structures with 4 to 6 w/o W additions, whereas with the previous N_2-H_2 atmospheres it was necessary to use the higher O/U ratio oxide (2.14) with 10 w/o W. Initial samples produced using this growth scheme were most interesting because the fiber density was significantly less (at equivalent growth rates) than those achieved using the $UO_{2.14}$ powder in the N_2-H_2 atmosphere. Preliminary calculations indicate a eutectic composition for UO_2-W (melted in a CO - 3000 ppm CO_2 atmosphere) of about 1.5 w/o W. Calculations of the eutectic composition of samples grown in the N_2-H_2 atmosphere typically have a eutectic composition of 3 to 4 w/o W. Thus it appears it may be possible to control (within limits) the

tungsten solubility (eutectic composition) through stoichiometry changes in the molten oxide in UO_2-W samples and provide more control over the pin array geometries which are emission tested. Figure 1 shows a UO_2-W sample with the low W concentration (1.5 w/o) with correspondingly larger pin spacings than those found in previous UO_2-W specimens.

Work is currently in progress examining the interrelationships of oxygen potential in the growth atmosphere, initial starting O/U ratio of the oxide and tungsten content on composite growth in UO_2-W samples, and more definitive results are anticipated after more data is available. One serious drawback was anticipated and encountered when the UO_2-W samples were lowered out of the rf coil without the molybdenum post-heater. Unusually severe thermal gradients were present in the solidified composite, and usually specimen crackings resulted. Efforts to decrease the thermal stresses during cooling are centered around using a platinum post-heater tube which will not react with the growth atmospheres.

3. Rare Earth Oxide-Metal Systems

As reported in the previous Report[1], ordered eutectic structures have been achieved using Mo or W in conjunction with Gd_2O_3, La_2O_3 and Nd_2O_3. The best composites were grown from these systems when the metal solubility was increased by the addition of ceria. The work in this area during the past six months has been concentrated on the Gd_2O_3-CeO_2-metal

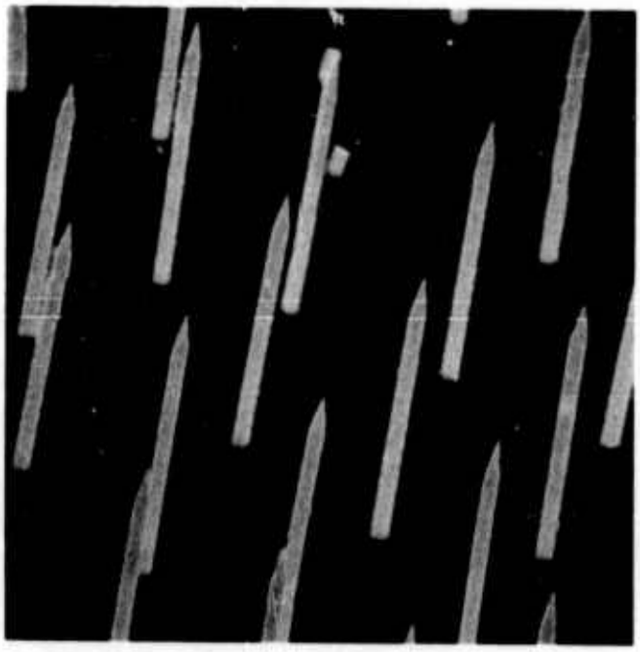

Figure 1. Scanning Electron Micrograph of UO_2-W Composite Containing Approximately 1.5 w/o W Displaying Widely Spaced Fibers.

system to avoid the hydration problems associated with La_2O_3 and Nd_2O_3. In addition, the use of CeO_2 as a matrix material for Mo was also investigated.

a. Gd_2O_3-CeO_2-Mo

The variation of fiber density and fiber diameter versus growth rate have been determined for the Gd_2O_3-20 m/o CeO_2 - 10 w/o Mo composition. Fiber density versus growth rate varied in a near linear manner as shown in Figure 2 for growth rates between 0.75 and 4.8 cm/hr. However, the parabolic equation

$$Y = 0.822 + 11.9X - 0.741\ X^2$$

where Y is the fiber density per cm^2 in millions and X is the the growth rate in cm/hr had a higher correlation coefficient (0.966) and a lower standard error of estimate (2.61×10^6 fibers/cm^2) than did the best linear fit for these data points.

The relationship between fiber diameter and growth rate is also parabolic in nature and is described by the equation

$$Y = 0.966 - 0.376X + 0.045X^2$$

where Y is the fiber diameter in microns and X is the growth rate in cm/hr. The correlation coefficient for this equation was 0.990, and its standard error of estimate was 0.031 microns.

Metal morphology and cell size versus growth rate and cell size versus growth length have been qualitatively determined in the Gd_2O_3-Mo system. The number and size of platelets decreased significantly as the growth rate was increased.

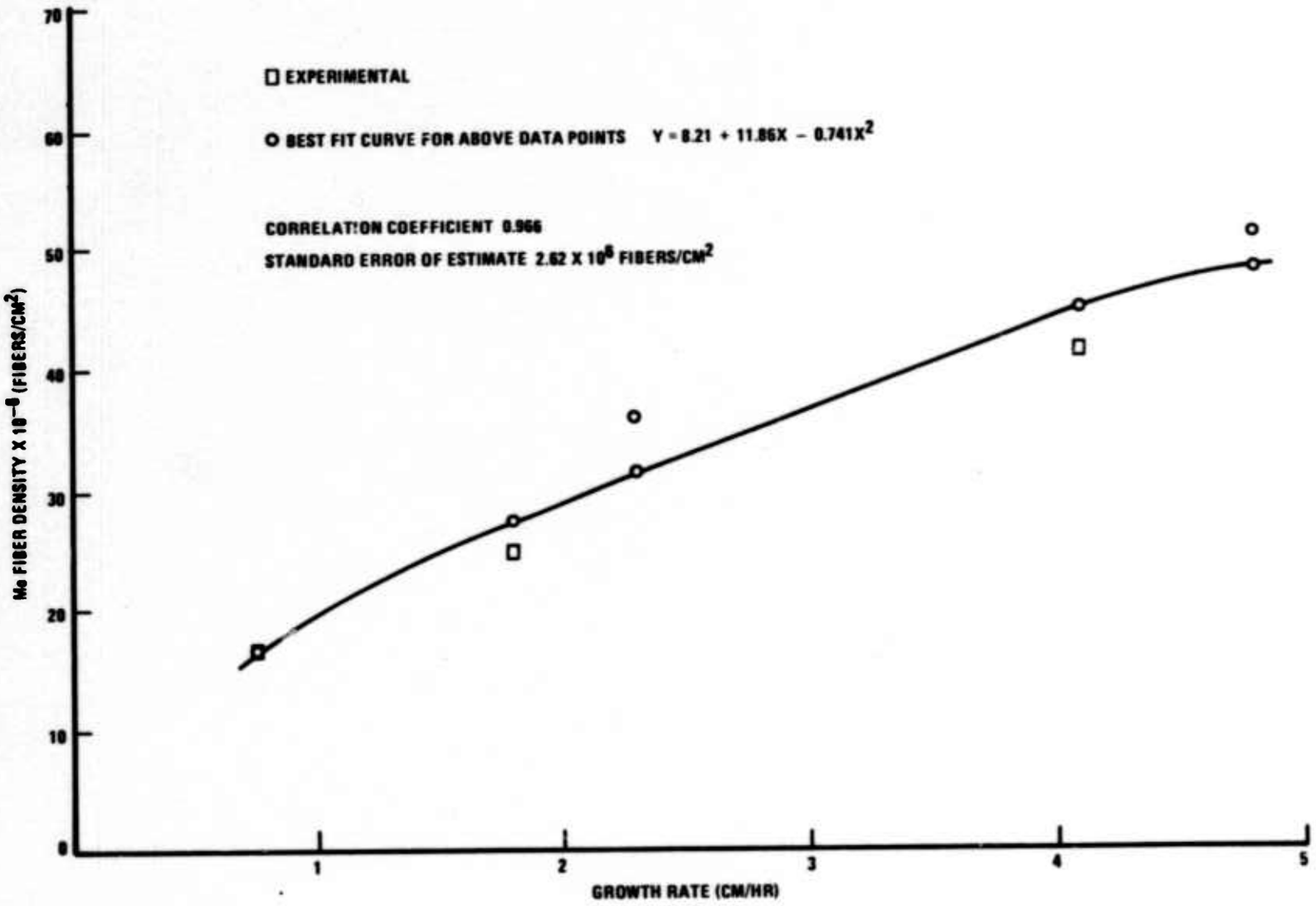

Figure 2. Effect of Growth Rate on Molybdenum Fiber Density in Gd_2O_3-CeO_2-Mo Composites.

However, samples grown at rates of 3.5 cm/hr and greater exhibited areas of disordered growth (similar to those observed in samples where the molten zone spontaneously travelled to the top of the pellet), and these disordered areas increased in size as the growth rate increased. A sample grown at 5 cm/hr had this disordered morphology (see Figure 3) throughout the entire solidified zone.

Figure 4 shows the typical microstructure of a Gd_2O_3-Mo sample grown at 4 cm/hr. Platelets are only present at cell boundaries, and no cell contains only platelets. However, when the growth rate was reduced to 2 cm/hr (see Figure 5), some cells contained almost entirely platelets and most cells contained a few platelets in their interiors. Cell size appeared to increase with growth length and decrease with increasing rate of growth.

The advantages of growing longer samples include larger cell size and more uniform growth the longer the length of the solidified zone. The more preferentially orientated cells will tend to predominate, and initial melt innomogeneities will tend to be damped out. It was felt that the high sintered density of the rare earth samples would permit composite growth up to 15 cm in length, since the void size (the main factor limiting growth in other systems) would not be a problem.

However, the maximum rod length that could be uniaxially pressed was about 5 cm. If longer rods were pressed, the middle of the rod was compacted less than the ends, so that

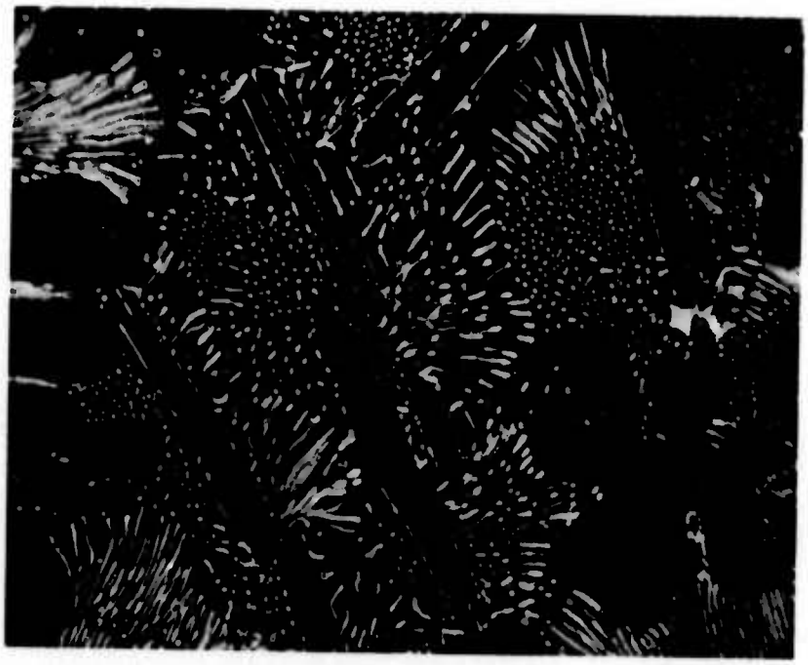

Figure 3. Disordered Composite Morphology of CeO_2 Doped Gd_2O_3-Mo Sample Grown at 5 cm/hr. Dark Field, X600.

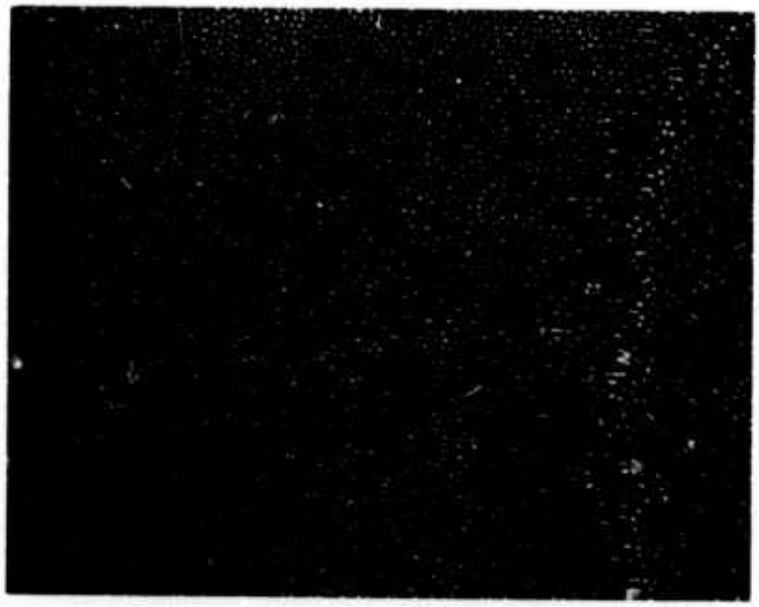

Figure 4. CeO_2 Doped Gd_2O_3-Mo Sample Grown at 4 cm/hr Displaying Mo Fibers in the Cell Interior Which Gradually Grade to Platelets at the Cell Boundary. Dark Field, X600.

Figure 5. CeO_2 Doped Gd_2O_3-Mo Sample Grown at 2 cm/hr Showing Cells Essentially Composed of Narrow Mo Platelets. Dark Field, X800.

when it was sintered prior to melting, it had an "hour glass" shape. Since the rf coupling efficiency decreases with decreasing diameter, the power requirements to keep a stable molten zone changed as the sample was lowered, making it very difficult to solidify the entire length of the pellet. When small pellets were stacked on top of one another to produce a longer sample, the fiber growth was disrupted when the molten zone moved through the interface between the pellets.

The use of thick walled rubber molds and isopressing technique allowed longer uniformly dense rods to be produced. Using these rods unidirectionally solidified lengths from 4 to 5 cm long were easily produced (see Figure 6). Even longer samples could be produced if the growth-lowering apparatus had a greater stroke length.

When the molten zone was passed through a Gd_2O_3-CeO_2-Mo sample twice in an attempt to improve fiber geometry, the fiber geometry was very poor with many Mo dendrites in the solidified area. This may be the result of the depletion of the oxygen from the CeO_2 during the first pass and the reduction of Mo solubility during the second pass.

b. Gd_2O_3-CeO_2-W

Long (4 to 5 cm) composite areas were difficult to produce in Gd_2O_3-CeO_2-W samples which had been prepared by isostatic pressing. The primary problem was that it was difficult to control the rf generator power so as to maintain the molten zone without decoupling or melting out through the sample skin.

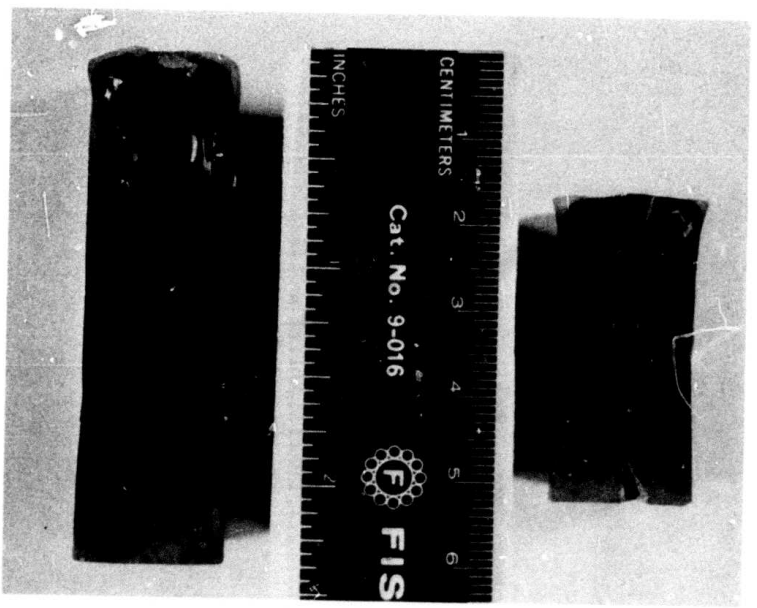

Figure 6. Comparison of the Size of CeO_2 Doped Gd_2O_3-Mo Composite Samples Initially Prepared by Uniaxial Pressing in a Steel Die (Right Pellet) and Iso-Pressing in a Rubber Mold (Left Rod).

When the molten zone was successfully passed through a sample containing W at 2.8 cm/hr, the disordered morphology seen in Mo samples at high growth rates was observed. This seems to indicate that ordered structures in the Gd_2O_3-CeO_2-W system may only be obtained at slower growth rates ($\sim$1 cm/hr).

c. CeO_2-Mo

Ceria - 10 w/o Mo samples have been successfully internally melted and unidirectionally solidified to produce ordered oxide-metal structures composed of metal fibers and lamella in the oxide matrix. Preliminary experiments indicate that CeO_2-Mo composites grown in a pure H_2 atmosphere contain only fibers, while samples grown in H_2-N_2 atmospheres (typically 10% H_2 - 90% N_2) contained half fibers and half lamella. The fiber areas in the samples grown in hydrogen are less uniform in size and spacing than the fiber areas in the H_2-N_2 grown samples. Figure 7 shows typical structures of the CeO_2-Mo samples grown in the N_2-H_2atmosphere.

Pure ceria composites differ from the predominantly sesqueoxide rare earth composites (Gd_2O_3-CeO_2, Nd_2O_3-CeO_2) in the following ways: 1) minimum preheat temperature is 30 to 40% lower; 2) pure ceria composites can be coupled to by separating the Mo preheater tubes in a manner similar to the technique used for UO_2; 3) ceria composites are much more susceptible to thermal shock; 4) ceria composites do not hydrate; and, 5) little sintering occurs during preheating.

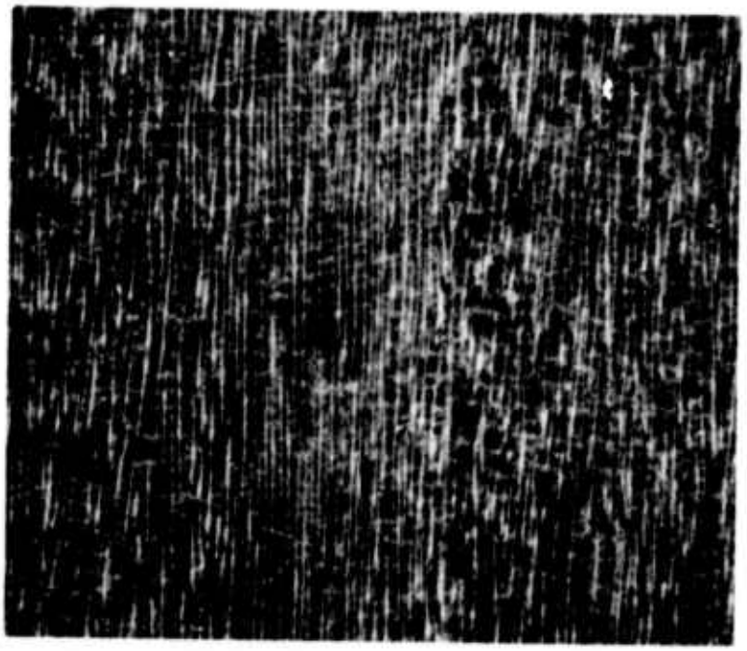

a) Fiber Growth.

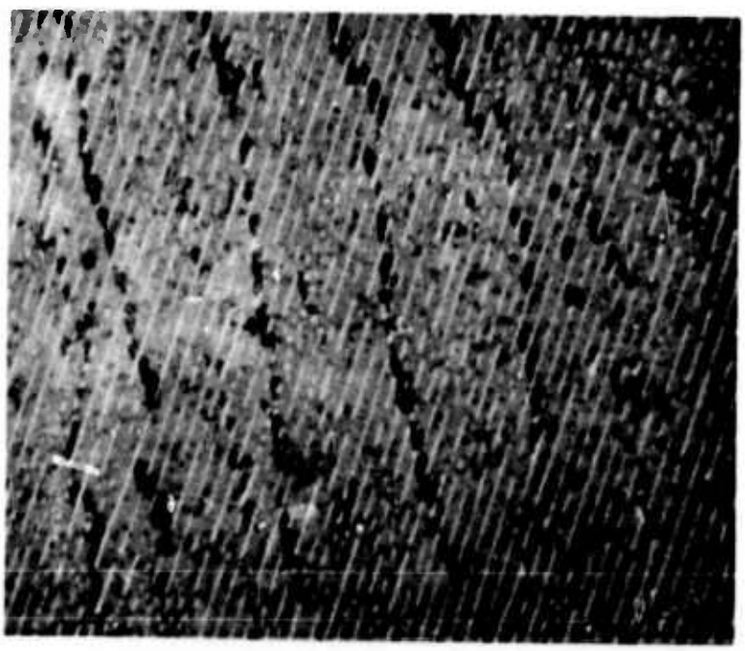

b) Platelet Growth.

Figure 7. Longitudinal Section of CeO_2-10 w/o Mo Samples Unidirectionally Solidified in a N_2-H_2 Atmosphere. Dark Field, X600.

The ability to form oxide-metal composite structures using CeO_{2-x} as the oxide component suggests that non-stoichiometric compounds may be more ideally suited than previously thought to form homogeneous molten metal-oxide mixtures. The potential unique feature with CeO_2 is that its oxide-metal eutectic temperature is significantly below that obtained with the current oxides under investigation, and consequently CeO_2 is considered a possible host for a variety of the lower melting metals. Additional work in this system is in progress.

4. $Al_2O_3(Cr_2O_3)$-W or Mo

Alumina would be an attractive matrix material for oxide-metal composites; however, previous efforts to induction melt this material have been unsuccessful because of the inability to impart enough electrical conductivity for eddy current heating. Two different techniques were employed this report period for melting Al_2O_3-W or Mo mixtures using direct rf heating, but unfortunately there was little if any apparent solubility of the refractory metals in the molten Al_2O_3.

In the first trials Al_2O_3 samples doped with 80 w/o Cr_2O_3 and mixed with 20 w/o W were preheated to 1800°C in N_2-H_2 atmospheres and then exposed to a 4 MHz rf field. Some internal melting was achieved, but it was difficult to maintain a stable molten zone. The second approach used molybdenum cylinders fabricated from 0.010" molybdenum sheet centered inside uniaxial pressed pure Al_2O_3 rods. These samples were preheated in a N_2-H_2 atmosphere to 1800°C to increase the conductivity

of the sample enough to form an internal molten zone when exposed to the 4 MHz rf field. Examination of several samples after melting all revealed a porous oxide phase suggesting the melt was "frothy". The Mo was in the form of large droplets indicating limited if any solubility of the metal in the molten alumina.

B. EFFECT OF LOWERING RATE ON THE EUTECTIC COMPOSITION OF UNIDIRECTIONALLY SOLIDIFIED OXIDE-METAL MIXTURES

As has been reported in this and previous reports, the fiber density and fiber diameter of unidirectionally solidified oxide-metal composites vary with growth rate. If the eutectic composition for a given system was independent of growth rate, the volume percent metal calculated by determining the product of fiber diameter and fiber density should be a constant for different growth rates. This has not proven to be the case in several oxide-metal systems.

The volume % Mo contained in the eutectic composition of CeO_2 doped Gd_2O_3 samples at five different lowering rates was found to follow the parabolic equation

$$Y = 8.927 - 3.500X + 0.3947X^2$$

where Y is the volume % Mo, and X is the growth rate in cm/hr. A plot of this curve and the experimentally determined Mo v/o is shown in Figure 8.

Similar analyses using UO_2-W data[3] and Y_2O_3 stabilized ZrO_2-W data[1] show that their eutectic compositions also vary

with growth rate and fit parabolic equations (see Figures 9 and 10). Their correlation coefficients and standard estimate of error were respectively R = 0.998, SEOE = 0.0272 v/o W and R = 0.707, SEOE = 0.452 v/o W. It should be noted that both the UO_2-W and Y_2O_3 stabilized ZrO_2-W best fit curves show the v/o W of the eutectic composition decreasing to a minimum with increasing growth rate and then increasing with further increases in growth rate. The calculated best fit curve for the v/o Mo in the Gd_2O_3-CeO_2 system eutectic also shows this trend, but samples grown at rates faster than 4.8 cm/hr are needed for confirmation. Using present growth techniques, fibers cannot be grown in this system at growth rates of 5cm/hr or faster.

Since results for the UO_2-W, Gd_2O_3-CeO_2-Mo and ZrO_2-Y_2O_3-W systems seem to suggest that eutectic composition varies with growth rate, the v/o W in a HfO_2-W sample lowered at 0.5 cm/hr and an identical one lowered at 1 cm/hr were calculated. The 0.5 cm/hr sample contained 12 million 0.37 micron diameter fibers/cm^2 and the 1 cm/hr sample contained 72 million 0.15 micron diameter fibers. This is equivalent to 1.29 and 1.27 v/o % W respectively. From this limited amount of data it is difficult to determine if growth rate affects the eutectic composition in the HfO_2-Y_2O_3-W system.

No explanation for the eutectic compositions to systematically vary with lowering rate has been determined, although several hypotheses will be investigated.

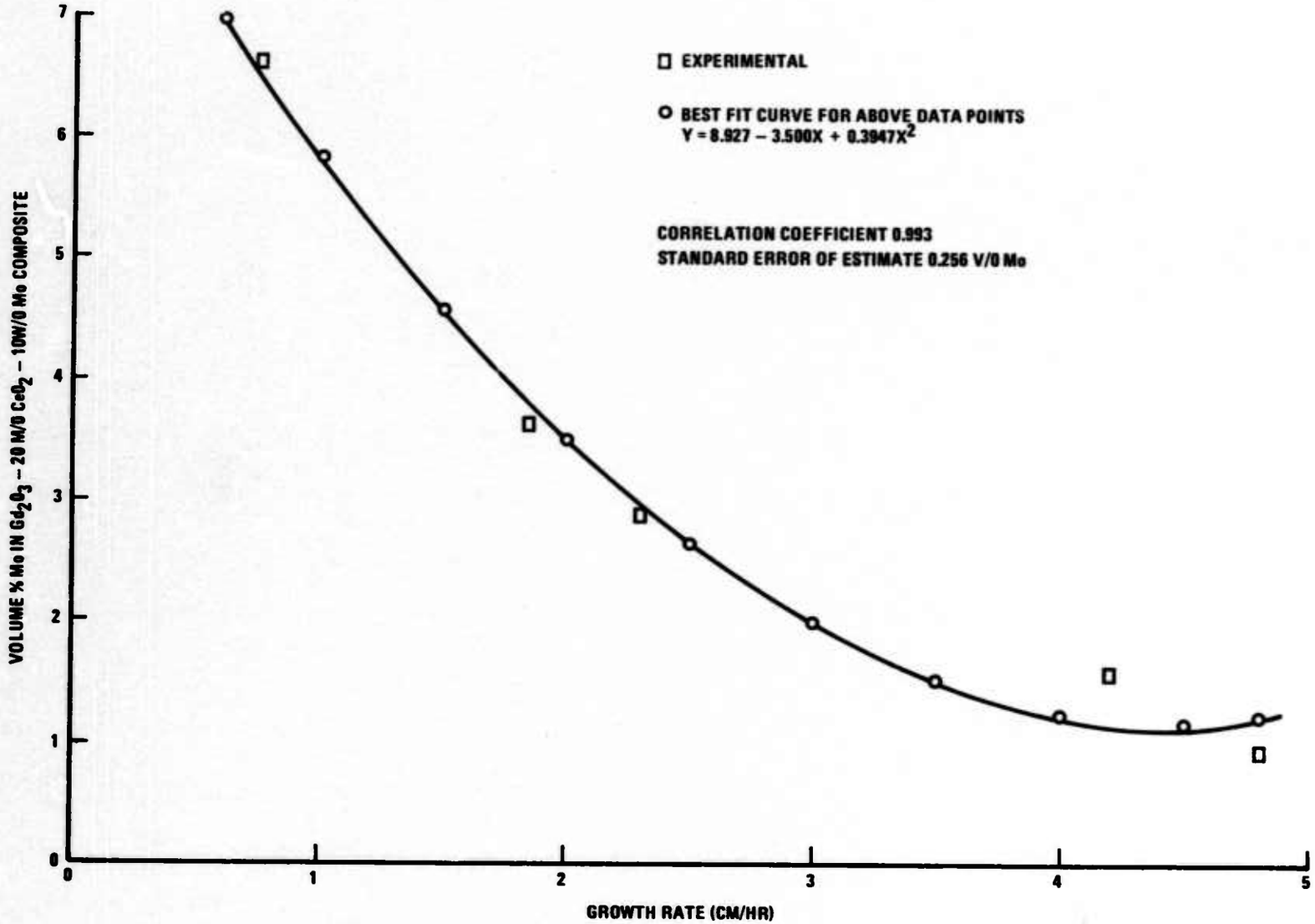

Figure 8. Effect of Growth Rate on v/o Mo Present as Fibers in Gd_2O_3-CeO_2-Mo Composites.

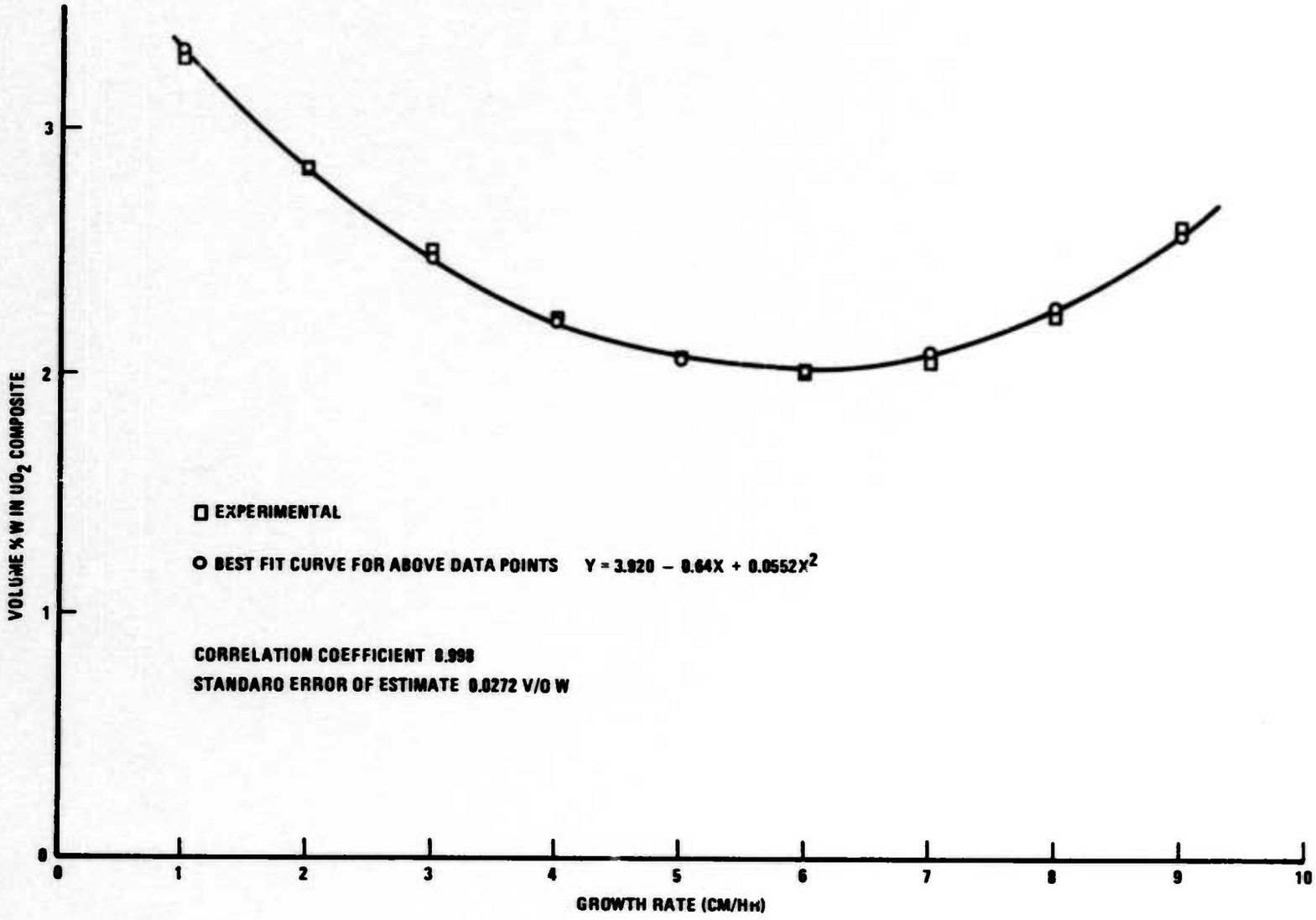

Figure 9. Effect of Growth Rate on v/o W Present as Fibers in UO_2-W Composites.

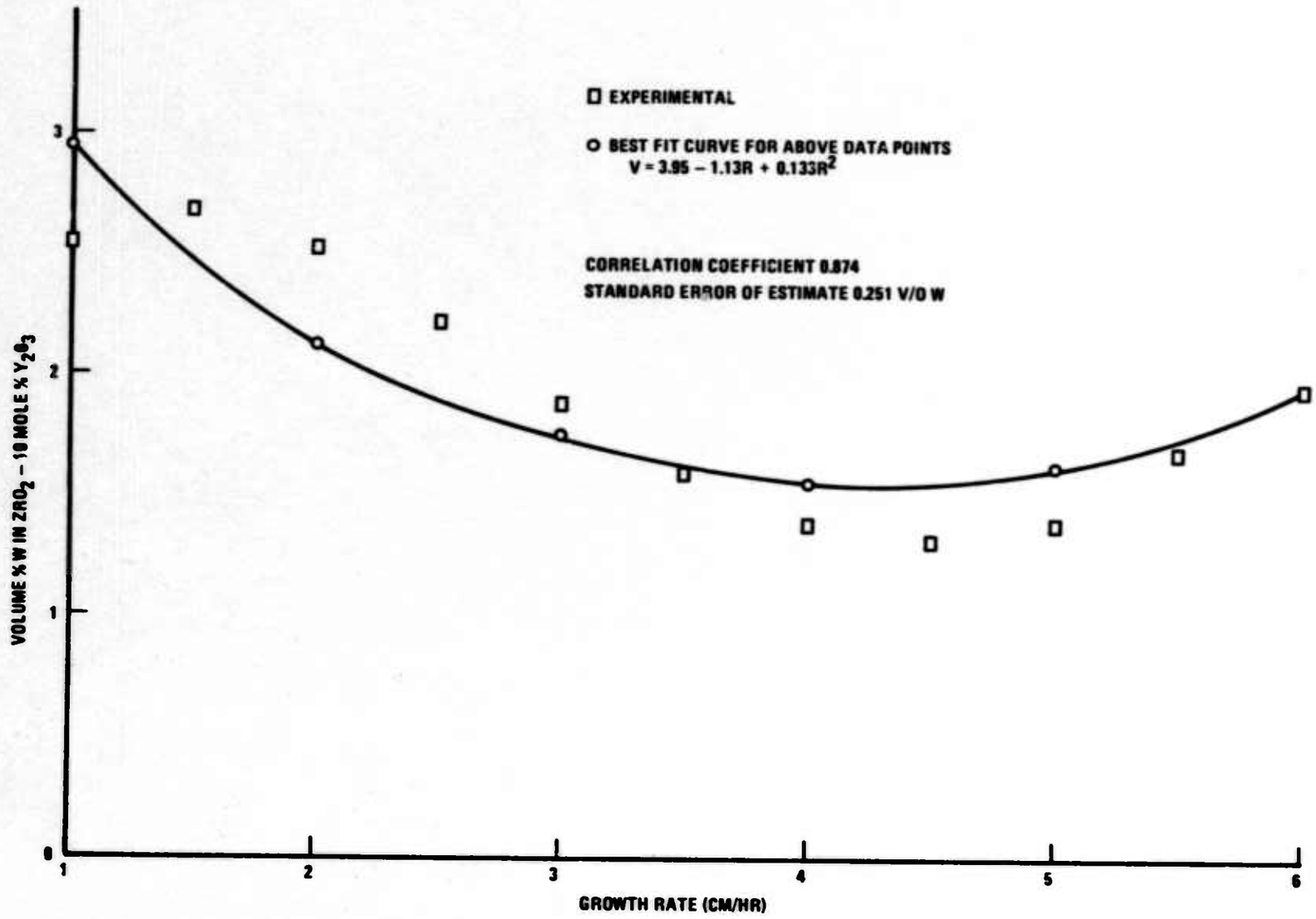

Figure 10. Effect of Growth Rate on v/o W Present as Fibers in ZrO_2-Y_2O_3-W Composites.

C. ELECTRON BEAM MELTING AND SOLIDIFICATION OF OXIDE-METAL SYSTEMS

A Materials Research Corporation electron beam zone refiner has been utilized in preliminary attempts to produce unidirectionally solidified eutectic composites in oxide-metal systems that cannot be inductively melted or cannot be successfully self-contained using the internal floating zone technique because of their low melting points.

The major portion of this contract period has been devoted to reworking portions of electron beam furnace that failed during use at high temperature and developing a technique for melting oxide-metal mixtures in crucibles formed from half-inch diameter Mo rods.

The originally supplied aluminum crucible support platform deformed during the electron beam welding of a top on a tungsten crucible and was replaced with a stainless steel platform. The steel roller bearings of the crucible rotating system were also welded to the crucible holder shaft and had to be replaced by a graphite sleeve bearing.

After these modifications were made a spinel ($Al_2O_3 \cdot MgO$)-10 weight % Mo mixture was heated above melting point of the spinel (2105°C) at which point a blown fuse terminated the experiment. Figure 11 is a micrograph of a polished cross section of this sample which shows the unmelted molybdenum particles surrounded by the solidified spinel matrix. The reason for the blown fuse was traced to vapor deposition of

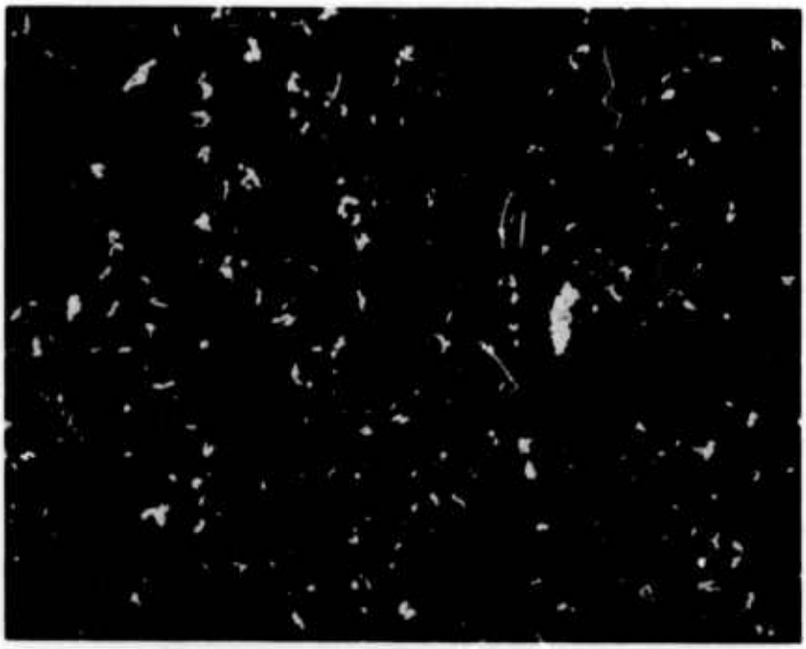

Figure 11. Solidified Region of $MgO \cdot Al_2O_3$-Mo Sample Showing Unmelted or Partially Dissolved Mo Particles. Bright Field, X200.

molybdenum from the crucible onto some of the high voltage electrical insulators which allowed current leakage to ground. This problem will most likely limit the maximum temperature to about 2000°C. Tungsten crucibles should allow considerably higher maximum temperatures to be reached.

The primary experimental problems associated with developing successful electron beam melting techniques still remain the difficulty in obtaining accurate temperature readings on the highly reflective crucible wall, just behind the hot tungsten filament, and an increase in crucible temperature as the thermal geometry changes as the hot zone is moved towards the top of the crucible. Experimental evidence indicates that correct power settings can be achieved by trial and error and monitoring the crucible's temperature about 5mm above the filament to reduce reflection problems.

D. X-RAY ANALYSIS OF OXIDE-METAL COMPOSITES

In previous reports[2,3,4] x-ray analysis of oxide-metal samples were reported for the systems UO_2-W and Y_2O_3 stabilized ZrO_2-W, with the major effort on UO_2-W samples. This section describes the initial x-ray analysis of CeO_2 doped Gd_2O_3-Mo composites and additional work on the other two systems.

Analysis of the as received commercial Gd_2O_3 powder using the x-ray diffraction diffractometer method showed the material to be cubic. However, in bulk composite samples No. 22-42 and No. 22-44, which were prepared by solidifying a mixture of 70 w/o Gd_2O_3, 20 w/o CeO_2 and 10 w/o W, the oxide was found

to have a monoclinic structure. The lattice parameters of the CeO_2 doped Gd_2O_3 were a_o = 14.17 Å, b_o = 3.59 Å, c_o = 8.83 Å and β = 100.1°, which are approximately 8% larger than the pure monoclinic Gd_2O_3 reported in the ASTM powder file. A powder sample No. 22-44/28-03, which was prepared by grinding Sample No. 22-44, was also studied by x-ray diffraction. By comparing reflections of the bulk (as grown) and powder samples, it was observed that the reflection peaks of the Gd_2O_3 of the bulk sample were much broader than that of the powder sample, and these reflections are shown in Figure 12. Since both small crystallite size and strain can broaden the x-ray reflection peaks, and the preparation of powder usually induces strain and decreases the crystallite size, the opposite effect shown in Figure 12 indicated that the bulk sample has a very high internal strain. This is probably partially produced by differential contraction of the matrix and metal fibers after solidification. These internal strains may also be magnified by a phase transformation occurring in the oxide matrix during the cooling. The information shown in Figure 12 indicates that this strain was partially released by grinding during the powder sample preparation.

Both melted and unmelted samples of ZrO_2 - 10 w/o Y_2O_3 were studied by the Debye-Scherrer method and found to have a fcc structure similar to zirconium (IV) oxide reported in the ASTM powder file. The lattice parameter was a_o = 5.14 Å, which is very close to that reported elsewhere[6]. The

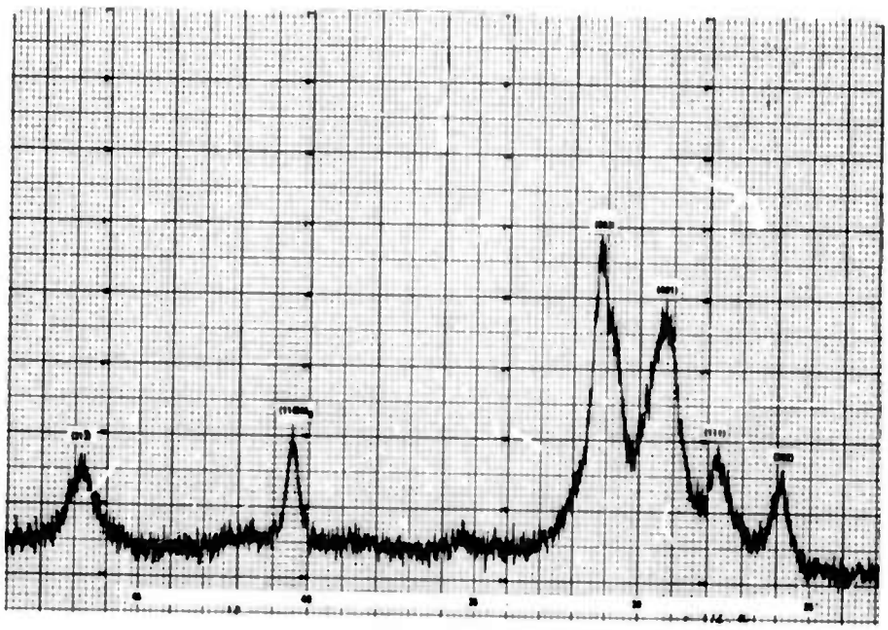

a) As-Grown Composite (Preferred Orientation Omits Some Reflections).

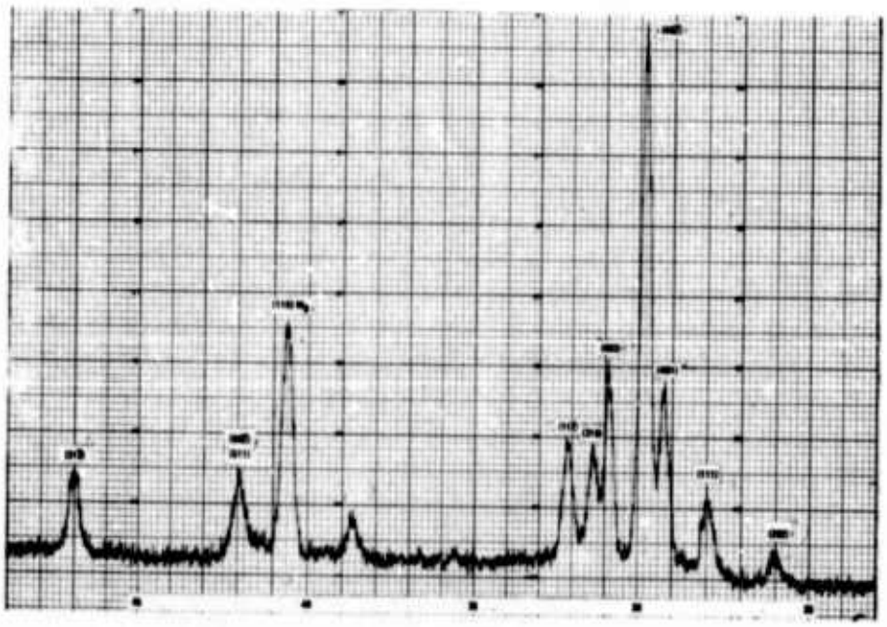

b) Powder Composite Sample After Grinding.

Figure 12. X-ray Diffraction Pattern of CeO_2 Doped Gd_2O_3-Mo Sample No. 22-44.

diffractometer x-ray diffraction examination of ZrO_2-Y_2O_3-W sample, No. 18-76, showed little if any internal strain in the matrix; however, the reflections from the tungsten fibers were considerably broadened, suggesting a strained condition.

The growth texture and orientation of ZrO_2-Y_2O_3-W sample No. 18-76 was also studied using (111) and (200) pole figure reflections of the ZrO_2-Y_2O_3 matrix and the (110) reflection of the tungsten fibers. The results showed that the matrix has a very slightly preferential [111] growth direction, which has been reported previously[2]. However, the intensity distribution of the (110) reflection from the fibers was rather random except for a slignt weaker intensity at the sample normal (which was the growth direction), and this conflicts with the earlier information.

In the earlier reports[2,3,4] the mutual orientation relationships of the fibers and matrix in the oxide-metal composites was reported using a single crystal orienter with the diffractometer. This method was used with the ZrO_2-Y_2O_3-W sample No. 18-76; however, no conclusive results were obtained, probably due to the small grain size of the sample. The Laue back reflection technique was used successfully for the study of the orientation relationships between the fibers and matrix in an additional ZrO_2-Y_2O_3-W sample. The x-ray beam size was 0.8 mm in diameter which was smaller than the average grain size of the ZrO_2-Y_2O_3-W sample, and the exact orientations of the fibers and matrix were determined simultaneously using slices cut perpendicular to the growth direction. Figure 13a

and 14a show the Laue back reflection patterns of two different grains (cells) of ZrO_2-Y_2O_3-W sample No. 18-76. The reflections of the ZrO_2-Y_2O_3-W grain shown in Figure 13a were distributed on the crystallographic zones, and the orientation was determined and shown in Figure 13b. The orientation of both the fibers and matrix are believed to be the same. Figure 14a shows the Laue pattern from the other grain. Both fibers and matrix reflections are clearly distinguishable. Their orientations are shown in Figure 14b. The [211] zone of the matrix are coincident with the [110] zone of the fibers, and the (111) of matrix and (110) of fibers are both on that zone with approximately 10° difference in orientation.

Figure 15 is the Laue back reflection of a UO_2-W composite, Sample No. 25-32, and the random distribution of the reflection spots on the photograph are probably due to the small grain size of the sample, less than the 0.8 mm diameter of the x-ray beam.

The mutual oxide-metal orientation relationships are important in the investigation of the nature of the metal-oxide interface. A series of Laue patterns will be taken in order to determine what orientation relations most frequently occur.

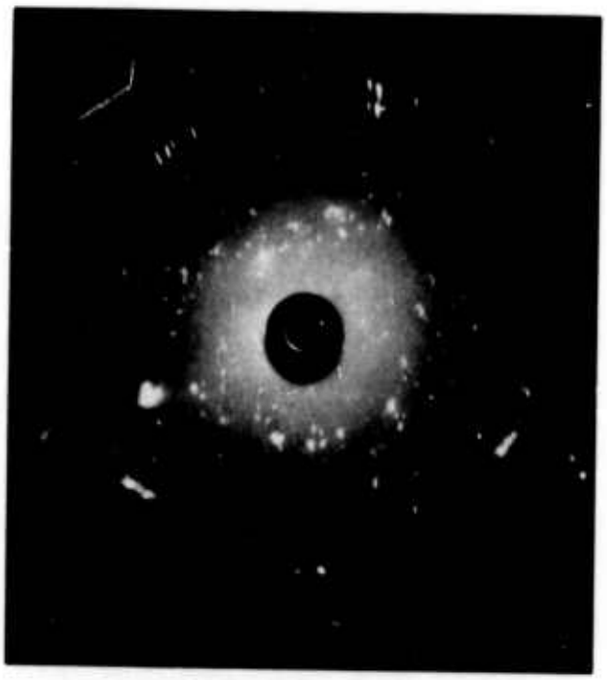

a) Laue Photograph.

#18 – 76

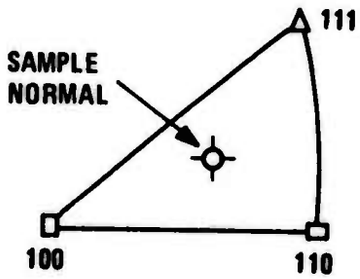

b) Orientation Relationship of Matrix and Fibers.

Figure 13. Laue Pattern of Y_2O_3 Stabilized ZrO_2-W Sample No. 18-76.

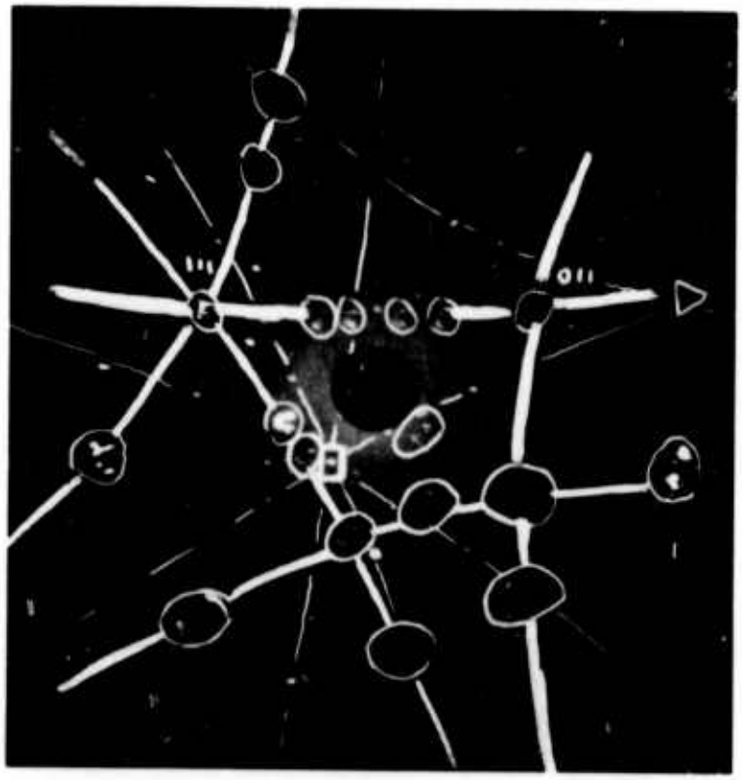

a) Laue Photograph.

MATRIX —o—

FIBERS ———

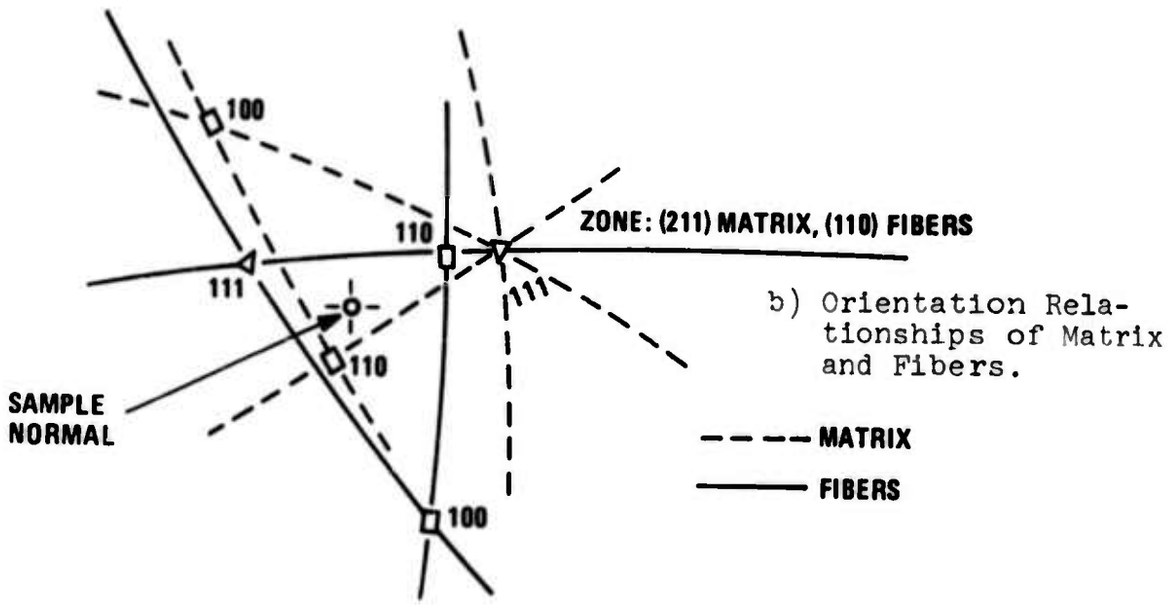

b) Orientation Relationships of Matrix and Fibers.

Figure 14. Laue Pattern of Second Area of Y_2O_3 Stabilized ZrO_2-Mo Sample No. 18-76.

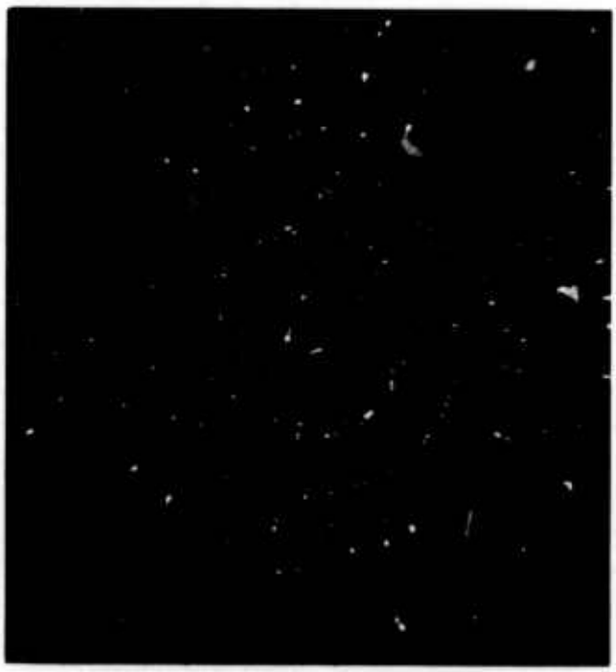

Figure 15. Typical Laue Pattern From UO_2-W Composite Sample No. 25-32.

SECTION III

FORMATION OF OPTIMUM EMITTING ARRAYS

During the past six months the principal areas of investigation designed to improve the emitting arrays have been the use of chemical etching techniques to shape the tips of exposed tungsten fibers in UO_2-W samples and the continued effort to improve the etching behavior of Gd_2O_3-Mo specimens. In previous work[1,2] the pointing of W pins was described; however, the repeatability was only fair because of the need for stringent control of the etching conditions. Because of this it was decided to perform a series of detailed UO_2-W etching experiments varying the etchant composition and temperature at which the etching was performed. The chemical etching apparatus was described in previous reports[1,2], and the variables of etching time and rotation speed were held constant at 30 minutes and 20 rpm respectively. These values were selected on the basis of previous work.

Initial experiments were performed using wafer shaped specimens from UO_2-W sample No. 113-6 in order to eliminate possible variables involved in different growth samples. In most cases a series of etching tests were made on the same pieces of material as prior tests, by simply repolishing the surface. In all cases the samples were prepared for etching by final polishing on 1 micron diamond paste..

Prior experimentation[1] had shown extremely good results in pointing fibers in UO_2-W samples using an etchant of the following composition at room temperature ($\sim 23^{\circ}C$).

20 ml saturated aqueous solution of CrO_3
10 ml glacial acetic acid
7 ml concentrated HNO_3
5.8 ml concentrated HF

In order to ascertain whether this composition constituted a good starting point for growth sample 113-6, a series of tests were made at $23^{\circ}C$, using the etchant noted above with HF contents of 5.0, 5.4, 5.8, 6.2, 6.6, and 7.0 ml. Results of this test showed a very definite increase in matrix roughness as HF content increased and the occurrence of extremely well pointed and uniformly shaped fibers at 5.8 ml HF. Figures 16a, b, c, d, e and f show typical results as the HF content increased from 5.0 to 7.0 ml.

The next step taken was to determine the effect of temperature when using the 5.8 ml HF etchant composition. Tests were performed at $48^{\circ}C$, $0^{\circ}C$, $-12^{\circ}C$, and $-90^{\circ}C$. At $48^{\circ}C$ pointed fibers of shorter taper were obtained, but the matrix was extremely rough and some fibers displayed surface roughening (see Figure17). At $0^{\circ}C$, $-12^{\circ}C$, and $-90^{\circ}C$ no etching or pointing of fibers was seen, but at $0^{\circ}C$ an extremely smooth matrix was produced (see Figure 18). At $-12^{\circ}C$ a smooth matrix was also obtained. However, the rate of attack on the matrix was slightly lower than at $0^{\circ}C$, and a time penalty would

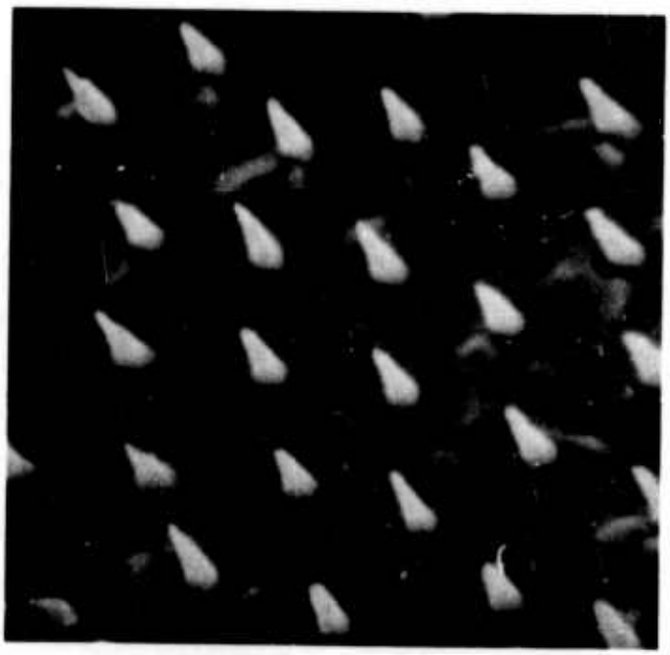

a) 5.0 ml HF.

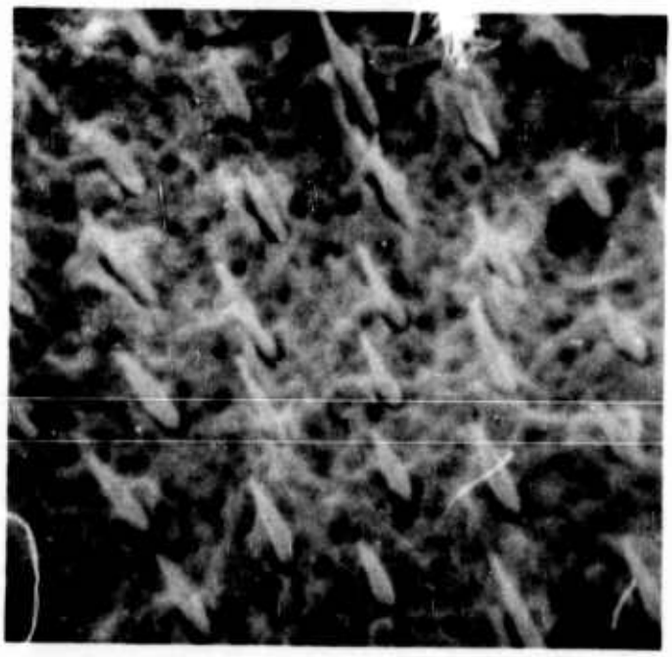

b) 5.4 ml HF.

Figure 16. Chemical Etching Behavior of UO_2-W Composites in Etchants of Varying HF Content. Scanning Electron Micrographs X10,000 - X12,000.

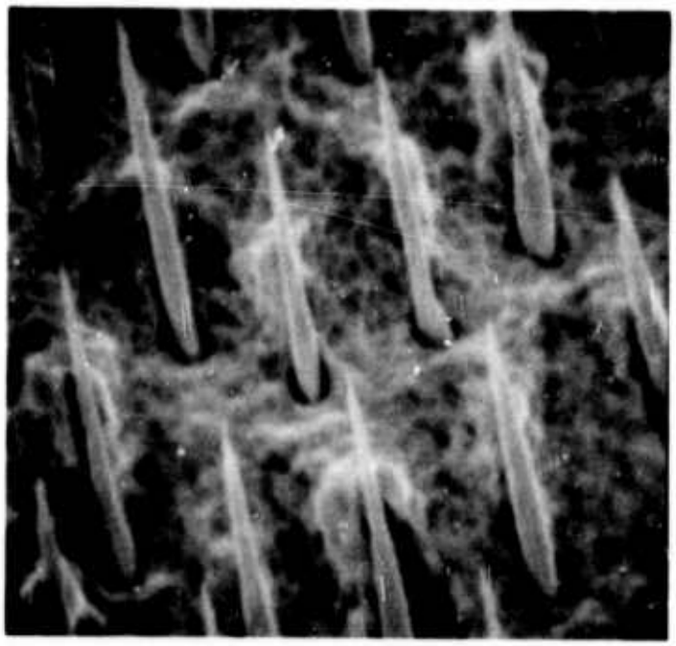

c) 5.8 ml HF.

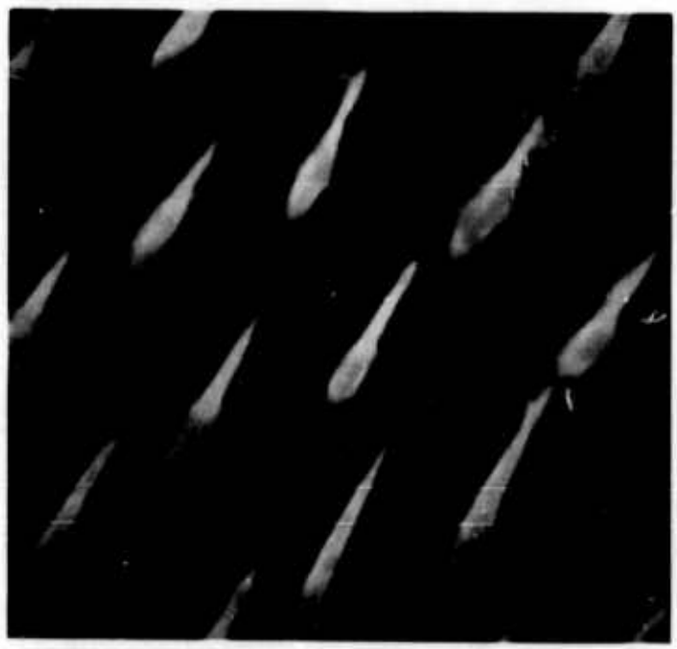

d) 6.2 ml HF.

Figure 16. (Continued).

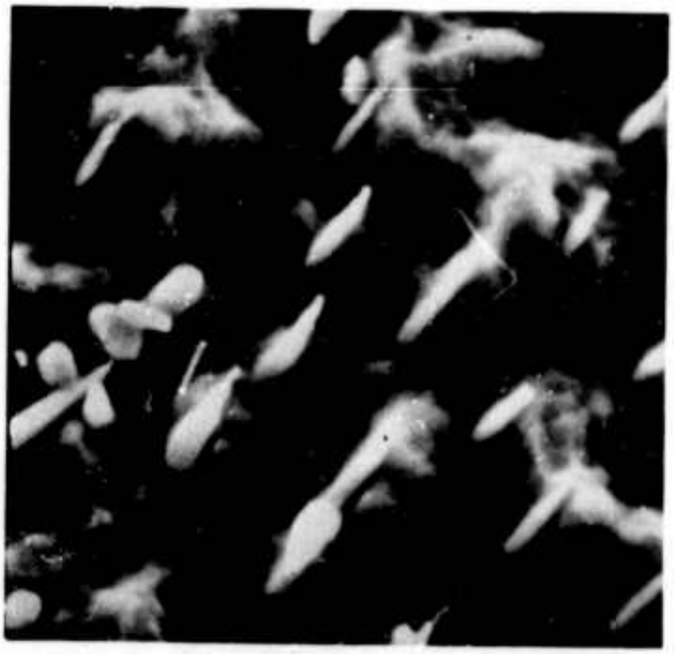

e) 6.6 ml HF.

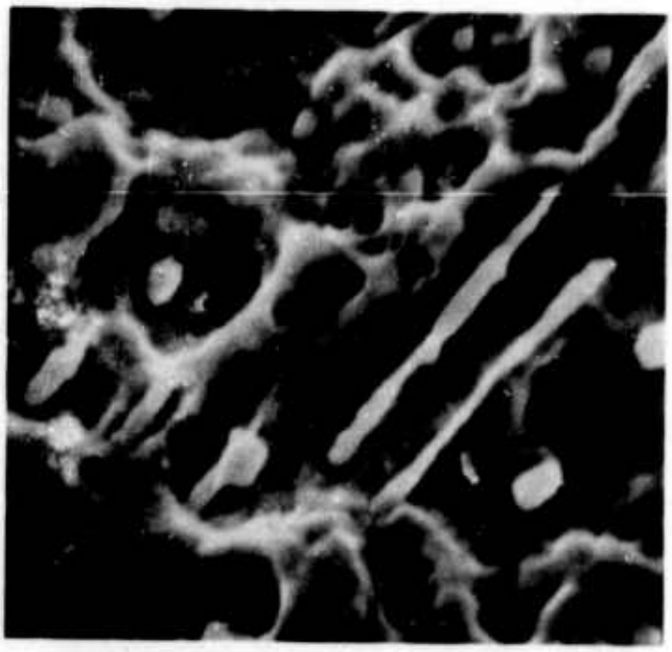

f) 7.0 ml HF.

Figure 16. (Continued).

Figure 17. UO_2-W Composite Etched at 48°C in Etchant Containing 5.8 ml HF. Scanning Electron Micrograph, X12,000.

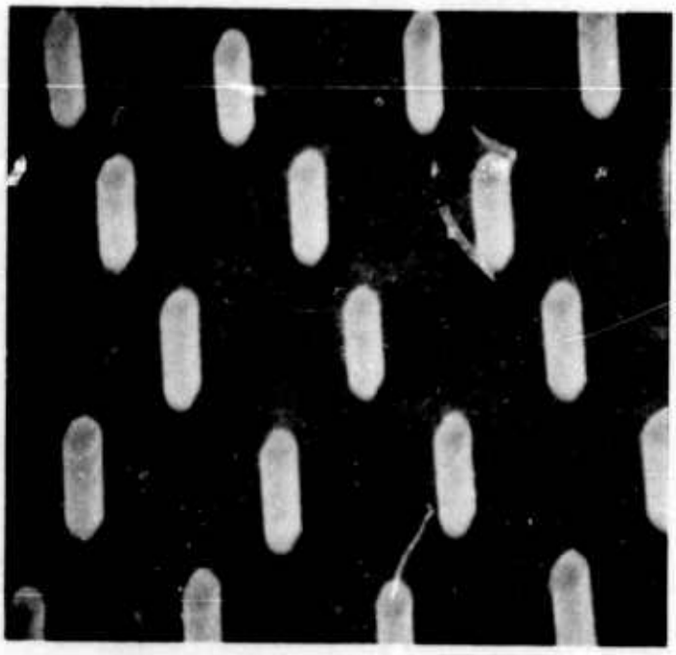

Figure 18. UO_2-W Composite Etched at 0°C in Etchant Containing 5.8 ml HF. Scanning Electron Micrograph, X12,000.

be incurred if etching were performed at this temperature (see Figure 19). At -90°C an unsuitable matrix morphology was observed with small dimples occurring in the oxide at the base of each fiber (see Figure 20). On the basis of these results, then, it was decided to continue with a series of tests at 0°C while again varying the HF content of the etchant.

Lower HF contents of 4.0 and 5.0 ml gave results which did not differ significantly from those obtained at 5.8 ml HF, as far as matrix quality and fiber length at 30 minutes etching time are concerned. As shown in Figure 21, increasing the HF content up to 6.6 ml HF produced no alteration of fiber shape but did slightly roughen the oxide matrix. A sample etched in a composition containing 7.4 ml HF showed very slight fiber modification and a very smooth matrix. Increasing HF content to 8.0, 9.0 and 10.0 ml produced gradual improvement of fiber pointing with no sacrifice of matrix quality until, at 10.0 ml, the fibers appeared very nearly identical to those produced by etching at 23°C with 5.8 ml HF content. The only difference noted was a slight roughening of the fiber surfaces in some instances, while the improvement in matrix finish more than offset this slight disadvantage (see Figure 22).

As noted above, an etchant containing 4.0 ml HF used at 0°C produced no fiber attack and an extremely smooth matrix. In the interest of producing pointed fibers of substantial length, it was felt that an investigation of this etchant's ability to produce long, undamaged fibers would be valuable

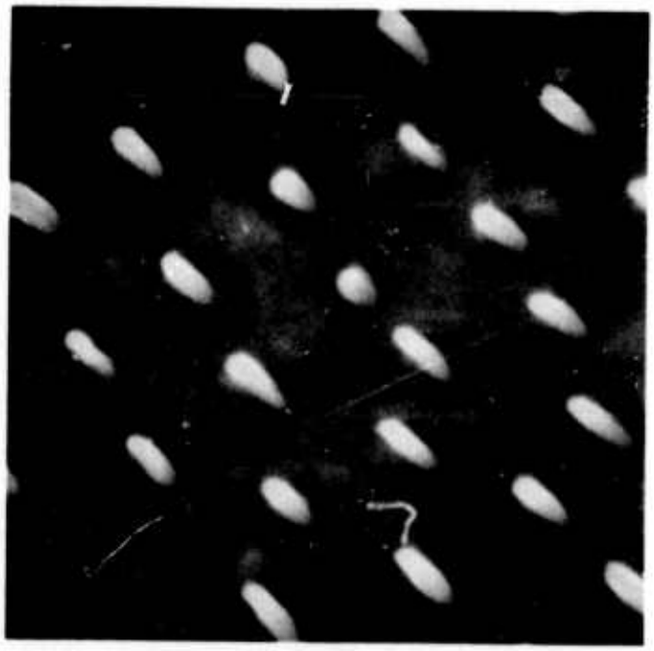

Figure 19. UO_2-W Composite Etched at -12°C in Etchant Containing 5.8 ml HF. Scanning Electron Micrograph, X11,000.

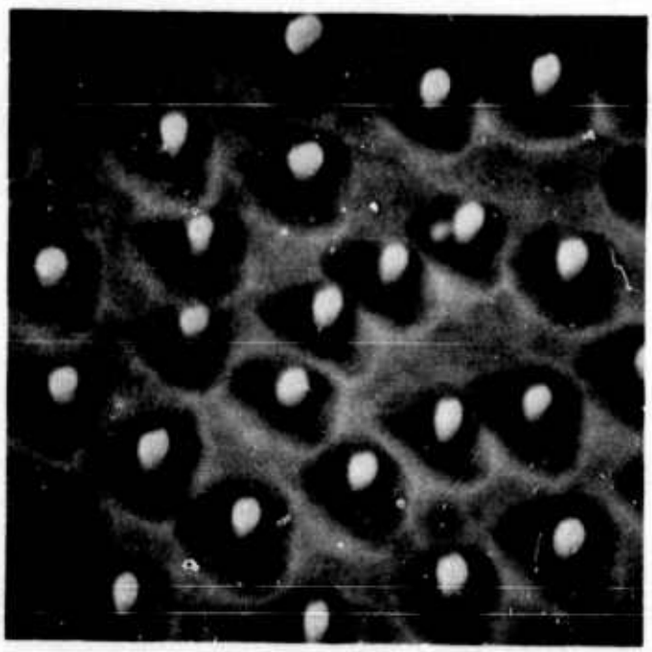

Figure 20. UO_2-W Composite Etched at -90°C in Etchant Containing 5.8 ml HF. Scanning Electron Micrograph, X11,500.

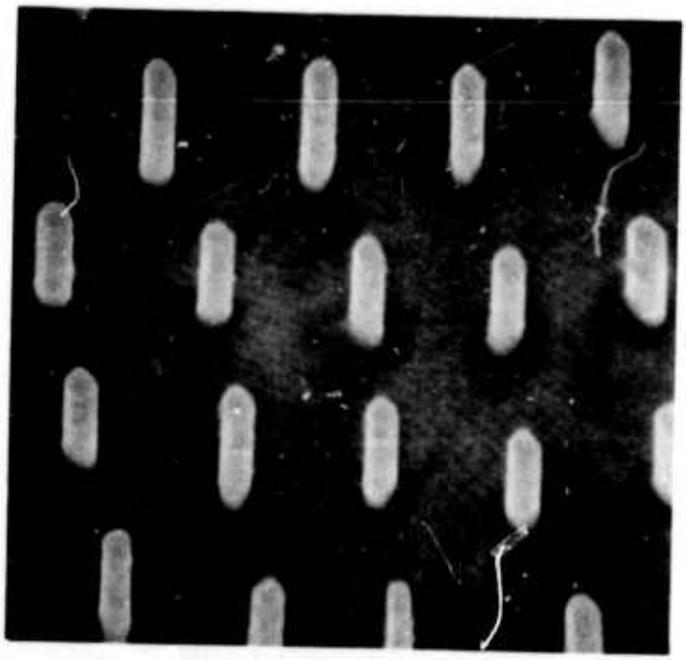

Figure 21. UO_2-W Composite Etched at 0°C in Etchant Containing 6.6 ml HF. Scanning Electron Micrograph, X12,000.

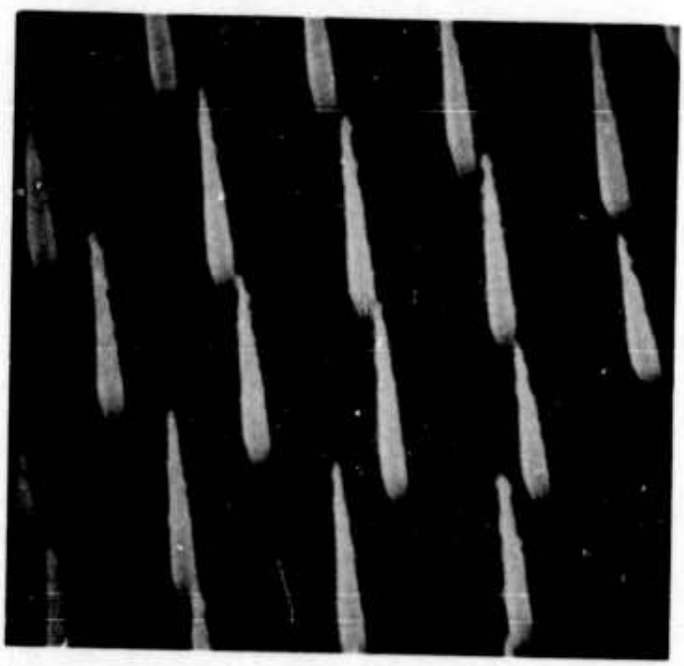

Figure 22. UO_2-W Composite Etched at 0°C in Etchant Containing 10.0 ml HF. Scanning Electron Micrograph, X11,000.

since it could be used in a two-step process, developed in earlier work[1], to produce desirable geometries for electron emission. A series of samples run for etch times of 15, 30, 60 and 120 minutes gave uneffected fibers of 1.42, 1.50, 2.04, and 5.12 microns in length, respectively. Figure 23 shows the results obtained with the etching time of 60 minutes. All samples in this series displayed an extremely smooth matrix surface and essentially undamaged fibers.

Further investigation of pointing fibers in UO_2-W samples was made in a series of experiments using an HF content of 10 ml and a reduction in the CrO_3 solution content from 20 ml to 15, 10 and 5 ml. Another objective being pursued was the ability to produce pointed fibers with an increased angle of taper (blunter points), and it was felt that this composition change might lead to progress in this direction. Figure 24 shows a sample etched at 0°C in an etchant of 10 ml HF and 15 ml of the CrO_3 solution; this composition produced pointed fibers of slightly increased taper at the expense of some slight roughening of the matrix. With 10 ml of the CrO_3 solution, a geometry never previously seen was obtained (see Figure 25). Around each pointed fiber there was a hole, and the tips of the fibers were nearly flush with the surface of the matrix. The holes had a diameter approximately three times that of the fibers and were of undetermined depth. Fiber points were not extremely uniform; some were very well tapered while others were only slightly rounded. The matrix surface

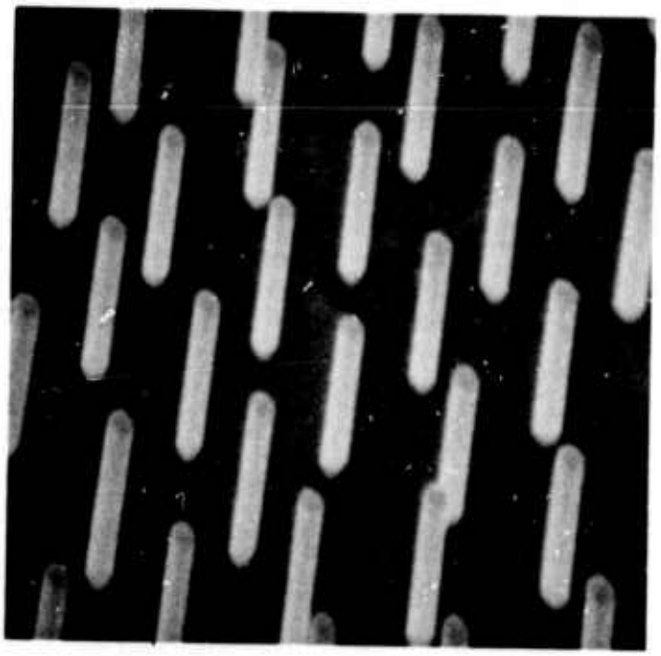

Figure 23. UO_2-W Composite Etched for 60 Minutes at 0°C in Etchant Containing 4.0 ml HF. Fiber Length Is Approximately 2 Microns. Scanning Electron Micrograph, X10,600.

Figure 24. UO_2-W Composite Displaying Blunter Points Obtained by Reducing CrO_3 Solution Content from 20 to 15 ml. Etching Was Performed at 0°C With HF Content of 10.0 ml. Scanning Electron Micrograph, X13,000.

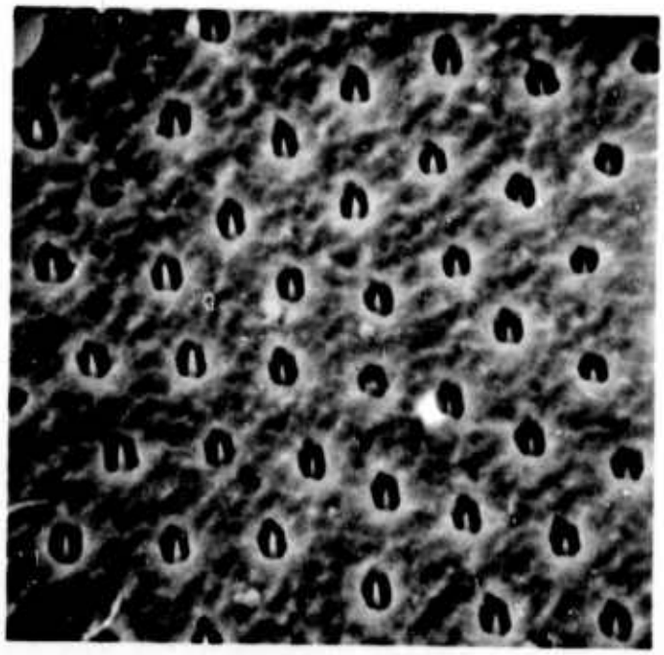

Figure 25. UO_2-W Composite Displaying W Pins Recessed in Oxide Matrix. Etching Was Performed at 0°C with 10 ml CrO_3 Solution Content and 10.0 ml HF Content. Scanning Electron Micrograph, X6,400.

outside the holes was somewhat roughened. The etchant composition with 5 ml of CrO_3 solution produced only very slight etching with no interesting effects.

Applying the information derived from the trials described above, the two-step etching process was employed in an attempt to produce long, pointed fibers with a more abrupt taper than those previously obtained. The first attempt used the following composition at 0°C for 30 minutes to point the fibers:

15 ml saturated aqueous CrO_3 solution
10 ml glacial acetic acid
7 ml concentrated HNO_3
10 ml concentrated HF
} pointing etch

and then the fibers were lengthened by etching for 30 minutes at 0°C in the second composition,

20 ml saturated aqueous CrO_3 solution
10 ml glacial acetic acid
7 ml concentrated HNO_3
4 ml concentrated HF
} lengthening etch

Good pointed fibers were obtained of about 3 microns in length using the first composition, and there was no noticeable damage to the points after treatment in the lengthening etch. Two more samples were prepared using the same etchants and procedure except that the lengthening etch time was extended to 60 and 90 minutes. Figure 26 shows the sample etched for 90 minutes. These tests produced longer fibers and maintained the sharply pointed tips. The greatest fiber length observed was 8 microns, and the taper of the tips was only very slightly greater than that of earlier samples. To determine the

reproducibility of the results, two more samples were etched as described above with lengthening times of 30 and 60 minutes. Fiber lengths for these samples were about 3μ and 6μ respectively. Matrix quality of all samples etched by the two-step process was very good.

One other experiment was performed using UO_2-W composite material from sample No. 113-6. A single sample was etched at $0^{o}C$ using the standard etchant for pointing the fibers (10 ml HF, 15 ml CrO_3, 7 ml HNO_3), but the glacial acetic acid content was reduced from 10 to 5 ml. Good fiber pointing was obtained on this sample, but the matrix quality was poor. Dimples were observed around each fiber, with a wave-like texture overlaying the depressions(see Figure 27).

Two additional experiments were performed using the etching techniques described above on UO_2-W sample No. 13-73 to check the reproducibility of etching characteristics between different growth samples. Two pieces were etched, one using the two step process with the pointing etch and a lengthening etch time of 60 minutes, the other using the etchant reported to give pointed fibers recessed in holes in the matrix. The first procedure gave fibers, with good pointed tips, about 4.5μin length. This is slightly shorter than the 6μ fibers reported for sample No. 113-6; the matrix quality was very good. The second sample gave very nearly identical results to those described previously for sample No. 113-6 and is shown in Figure 28.

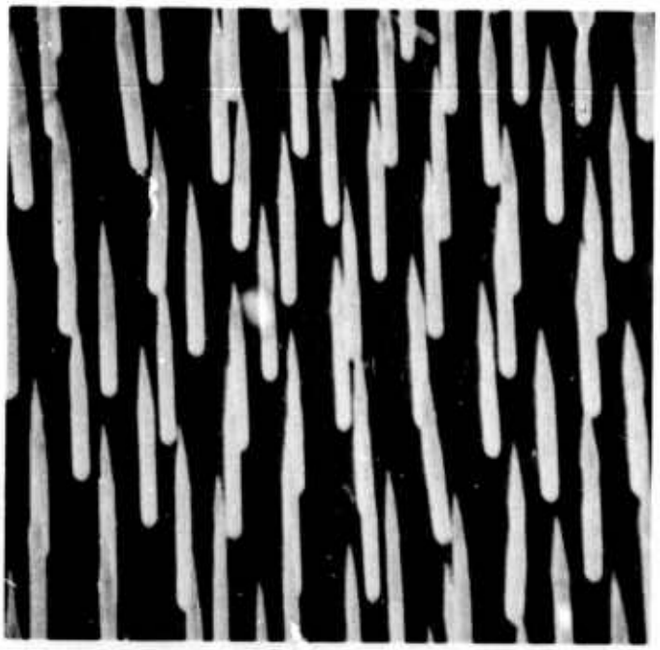

Figure 26. UO_2-W Composite Etched Using Two-Step Etching Procedure with 90 Minute Lengthening Etch Time. Fiber Length Is Approximately 8 Microns. Scanning Electron Micrograph, X5,700.

Figure 27. UO_2-W Composite Etched in Standard Pointing Etch at $0^{o}C$ with Glacial Acetic Acid Content Reduced from 10.0 to 5.0 ml. Scanning Electron Micrograph, X5,500.

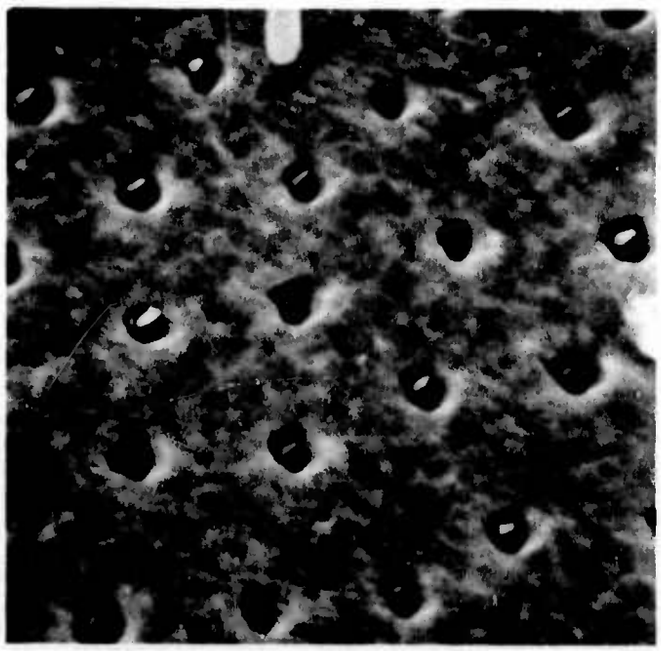

Figure 28. UO_2-W Composite (Sample No. 13-73) Etched to Demonstrate Reproducibility of Producing Pointed, Recessed Fibers in Various Growth Samples. Scanning Electron Micrograph, X12,500.

Previously reported investigations[1] have demonstrated the feasibility of using the ultrasonic cleaner to provide the required relative motion between etchant and the UO_2-W composite sample. This approach was applied in an effort to increase the rate of lengthening the previously pointed fibers and reduce the time required to achieve any desired fiber length. A first attempt using ultrasonic motion was made using the 7.0 ml HNO_3, 4.0 ml HF etchant composition which satisfactorily lengthened the fibers on a rotating sample at 0°C. The etchant temperature was maintained at 30°C, and etching time was 15 minutes. Examination of the sample showed that the matrix attack was extreme, leaving the oxide very rough; some attack on the fibers was also evident. The etchant composition previously used successfully in the ultrasonic cleaner, containing 3 ml HNO_3 and 2 ml HF, was retried and gave a smooth matrix and undamaged fibers at an etchant temperature of 24°C and etching times of 5 and 15 minutes. Figure 29 shows a typical UO_2-W sample etched with the 3/2 composition in the ultrasonic cleaner for 15 minutes. Note that the fiber lengths vary over the surface of the sample, and are longer near the edges and shorter in the interior of the sample. Due to this non-uniformity of etching characteristics, the ultrasonic method was discontinued, and an attempt was made to use the 3 ml HNO_3: 2 ml HF composition for the second lengthening etchant while rotating the sample at 20rpm. Figure 30 shows a UO_2-W sample prepared using the standard 0°C

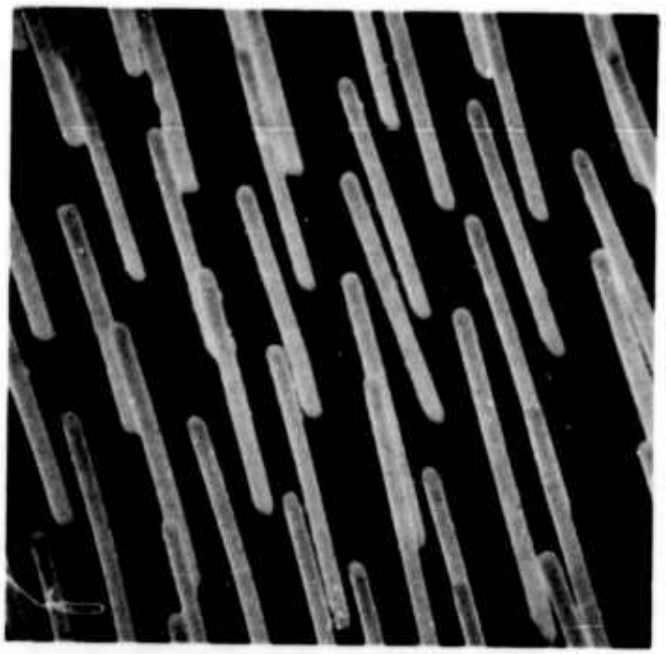

Figure 29. UO_2-W Composite Etched for 15 Minutes in Ultrasonic Cleaner Using 3 ml HNO_3:2ml HF Composition. Scanning Electron Micrograph, X6,500.

Figure 30. UO_2-W Composite (Sample No. 25-49) Showing Results Obtained by Lengthening Etch at Room Temperature Rotating Sample at 20 rpm. Scanning Electron Micrograph, X6,500.

pointing etchant followed by a 30 minute etching under the above conditions. It should be noted that this sample was produced from yet another UO_2-W growth specimen, No. 25-49; good reproducibility from sample to sample is indicated by these results.

Table II presents a summary of the chemical etching results obtained with CeO_2 doped Gd_2O_3-Mo composites. Initial investigations in this area using HCl as an etchant gave very poor results unless the etchant temperature was about -30°C. At this temperature, however, etching rates were extremely low, requiring 2 hours to obtain fiber exposures of a few microns. At or near room temperature an extremely rough matrix was obtained with very non-uniform etching of the Mo fibers.

Investigation of other etchants revealed that improved samples with essentially unaffected Mo fibers could be obtained using an etchant composed of 88% H_2SO_4 and 12% methyl alcohol. Etching was performed at room temperature, and significant fiber exposure was obtained with a rotating wafer-shaped sample in 15 minutes (see Figure 31).

An investigation of etchant composition designed to expose and point the Mo fibers (to achieve improved electron emission arrays) was also undertaken. Some modification of fibers was achieved by an addition of 10% HF to the H_2SO_4-methyl alcohol etchant; however, the matrix quality was very poor and pointing was not uniform with this etchant. Further work led to use of an etchant containing 96% H_2SO_4, 2% HNO_3, and 2% HCl. Etching

at room temperature for 10 minutes yielded Mo pin shapes shown in Figure 32. Fiber pointing in this Gd_2O_3-Mo sample was quite uniform, but the matrix quality still needs improvement. Work is continuing in this area in an attempt to produce Gd_2O_3-Mo emitting arrays comparable to those achieved with the UO_2-W composite materials.

TABLE II

SUMMARY OF CHEMICAL ETCHING BEHAVIOR OF Gd_2O_3-Mo COMPOSITES

Etch	Temp.	Time	Matrix	Fibers
HCl conc.	-30°	2 hours	smooth	Exposed. No attack.
HCl conc.	-10°	30 min.	fairly smooth	Exposed. No attack.
HCl conc.	0°	15 min.	rough	Exposed. No attack.
H_2SO_4-50%H_2O	RT*	15 min.	very rough	Exposed. No attack.
HNO_3-50%H_2O	RT	15 min.	very rough	Exposed. No attack.
Acetic Acid + 50% H_2O	RT	15 min.	no attack	Not exposed. No attack.
NaOH 50%H_2O	RT	15 min.	no attack	Not exposed. No attack.
Conc. H_2SO_4	RT	20 min.	smooth	Exposed. No attack.
H_2SO_4+10%Na_4OH	RT	20 min.	fairly smooth	Exposed. Some attack. No pointing.
H_2SO_4 + 12% Methanol	RT	20 min.	smooth	Exposed. No attack. (see Figure 31)
H_2SO_4-10% HF -12% Methanol	RT	20 min.	poor matrix	Exposed. Uneven attack. Some pointing.
Methanol - 12% H_2SO_4	RT	1 hour	fairly smooth	Exposed. No attack.
H_2SO_4-10% HF	RT	15 min.	fairly smooth	Exposed. No attack.
H_2SO_4-20% HF	RT	15 min.	fairly smooth	Exposed. No attack.
H_2SO_4-30% HF	RT	15 min.	fairly smooth	Exposed. No attack.
H_2SO_4-10% H_2O	RT	10 min.	fair	No attack.
H_2SO_4-1.1 w/o -NH_4NO_3	RT	10 min.	poor	Some tipping.
96%H_2SO_4-2%HNO_3 -2% HCl	RT	10 min.	poor	Good tipping. (see Figure 32)
H_2SO_4-1% HNO_3	RT	10 min.	poor	No attack.
H_2SO_4-1% HNO_3 -1% HF	RT	10 min.	good	Holes etched.
HF	RT	30 min.		No attack.

*RT = Room Temperature

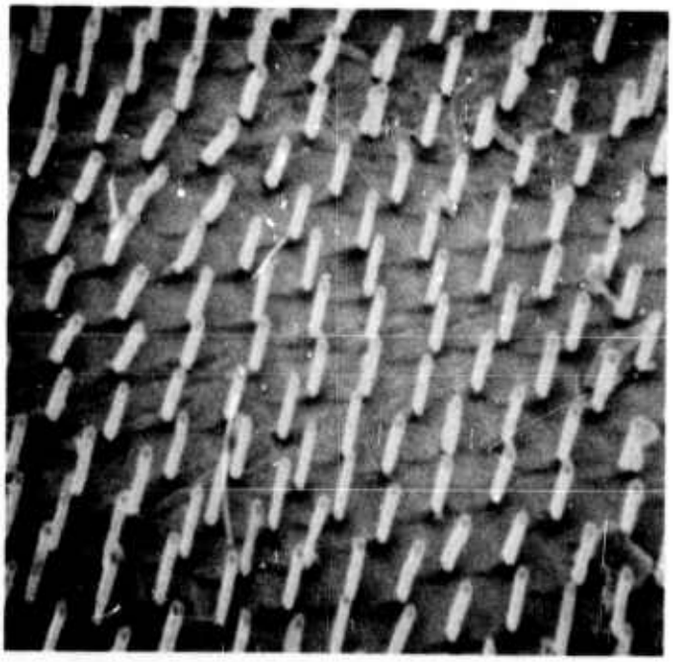

Figure 31. CeO_2 Doped Gd_2O_3-Mo Composite Etched in 88% H_2SO_4 - 12% Methyl Alcohol for 15 Minutes. Scanning Electron Micrograph, X5,200.

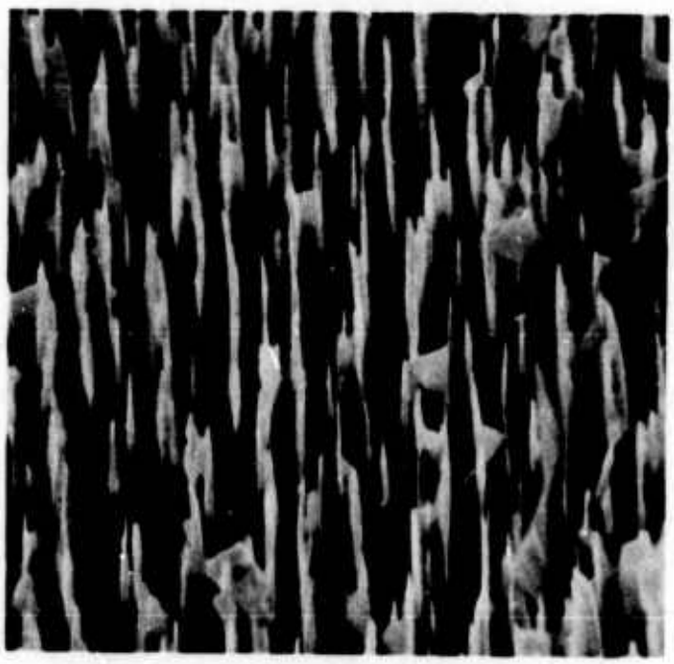

Figure 32. CeO_2 Doped Gd_2O_3-Mo Composite Showing Fiber Pointing Obtained with 96% H_2SO_4, 2% HNO_3, 2% HCl. Scanning Electron Micrograph, X5,550.

SECTION IV

OXIDE-METAL COMPOSITE PROPERTIES

In the previous report[1], the requirement to make a good electrical contact to the individual metallic fibers (pins) in oxide-metal samples used in emission testing was reviewed. Electrical resistivity measurements were accomplished using Hg and vapor deposited metallic-coatings as contacts, and these measurements were used as an estimate of fiber continuity in selected samples. SEM micrographs and electrodeposition methods showed about 70% of the fibers to be continuous in UO_2-W samples. During the present report period the brazing of composite samples to molybdenum discs with silver solder, platinum and copper was investigated, and the improved electrical contact achieved through brazing is thought to contribute to the improved electron emission performance reported in Section V.

A. SILVER SOLDER BRAZING

Four silver based solders were elected for the initial brazing experiments: ordinary wire type silver solder, 0.003 mil ribbon silver solder (type Na 50, 50% Ag), and Dupont 6320 and 6337 "fired-on" silver compositions. A Sessill drop test was performed with each braze by placing small amounts of the braze on a molybdenum disc, melting in a H_2 atmosphere and

observing the contact angle at room temperature. All the solders melted and flowed near 750°C. The brazes were ranked in order of decreasing wetting and increasing contact angle as follows: 1) ribbon silver solder and Dupont 6320 (contact angles approaching zero), 2) ordinary silver solder (contact angle 2-3°), 3) Dupont 6337 (contact angle 5-7°). The Dupont compositions showed some black residue probably due to too rapid a firing cycle causing carborization of any remanent organic binder. The firing cycle for the silver solders was not as critical as the firing cycle for the Dupont compositions, so the ribbon silver solder was selected for initial trials in making contact to the composites.

Composite samples were polished and etched to expose the pins prior to soldering. Possible oxide surface layers on the metal pins were removed before soldering by heating the sample and support structure to 1000-1100°C in H_2 for 10-20 minutes, and cooling to room temperature in H_2. After cleaning, solder was quickly placed between the composite and the supporting molybdenum discs or pins and the sandwich arrangement was heated to about 750°C for 5-15 minutes to allow the solder to flow. The sample was not removed from the H_2 until it had reached room temperature.

Visual inspection of the brazed samples revealed good melting and resistivity values were lower than those obtained using other contact methods. The bulk resistivity of UO_2-W sample #13-73/11-40/23-3, corrected for volume fraction of W

(3%), was 6.0×10^{-4} ohm-cm. The molybdenum discs brazed to this sample were pryed off and an inspection of the disc and sample was made in the SEM. The sample surface, Figure 33, revealed the broken ends of fibers in most areas and small areas where the fibers had remained in the matrix and pulled out of the braze. The broken fibers show necking, typical of metal tension failure. The braze surface, Figure 34, showed large areas of fibers embedded in the braze and necking was again evident. Holes in the braze were assumed to correspond to areas where fibers remained on the matrix. This evidence coupled with the low resistivity values obtained indicated that the braze had wet the tungsten fibers well.

A Gd_2O_3-Mo composite was also brazed to a molybdenum disc using silver solder. The bulk resistivity of Gd_2O_3 - 20% CeO_2-Mo sample 22-13/11-42/23-9, corrected for volume fraction of Mo (3%), was 2.6×10^{-3} ohm-cm. Before brazing to molybdenum discs, this sample was checked using mercury contact on a polished surface. Bulk resistivity measured 4.5×10^{-1} ohm-cm, or more than two orders of magnitude higher than measured with silver solder contact.

Several UO_2-W samples were brazed to molybdenum pins with silver solder for emission testing, and the emission performance improved over previous samples, partially due to better electrical contact achieved by brazing. Additional samples were brazed with silver solder; however, routine brazing with this material proved very sensitive to minor changes in

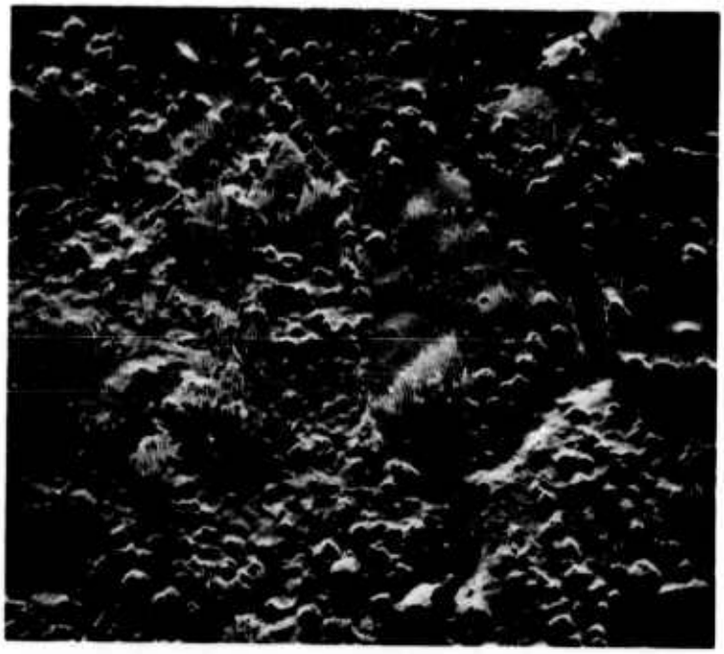

a) X 240.

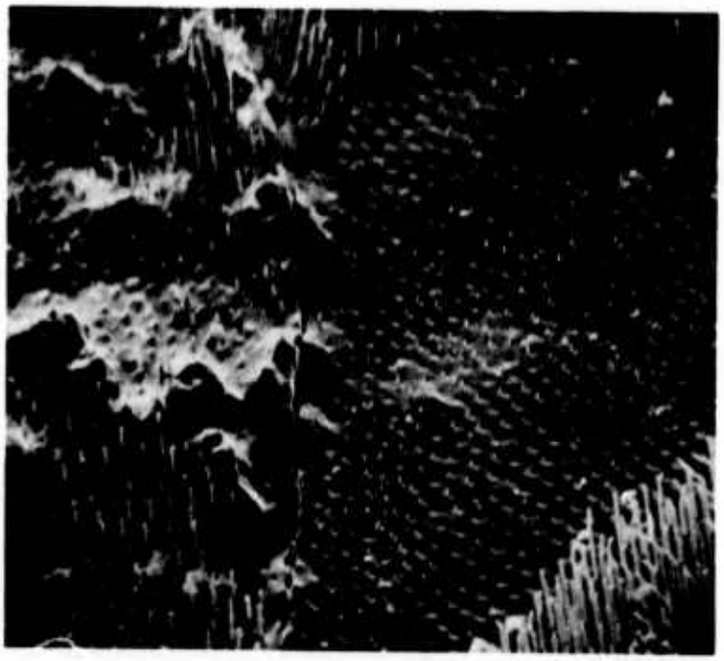

b) X 1200.

Figure 33. Surface of UO_2-W Composite After Prying Mo Disc-Composite - Mo Disc Sandwich Brazed with Silver Solder Apart. Scanning Electron Micrographs.

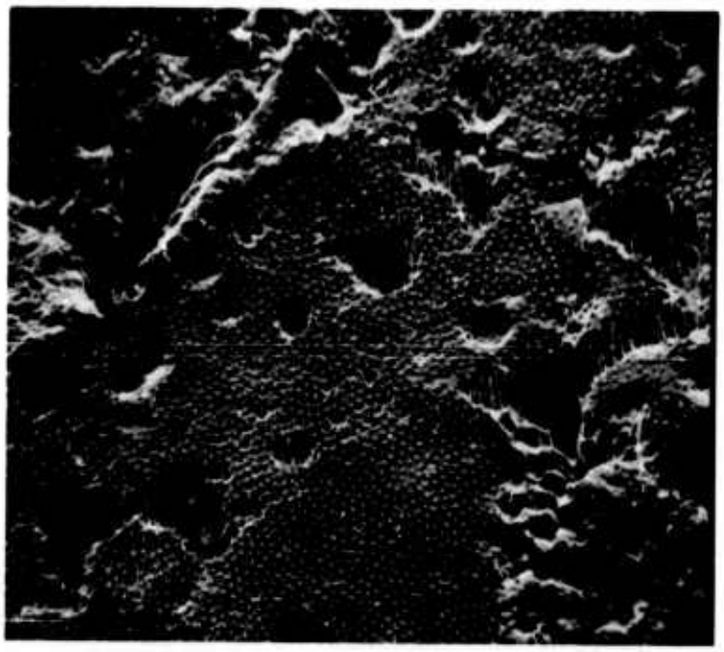

a) X 590.

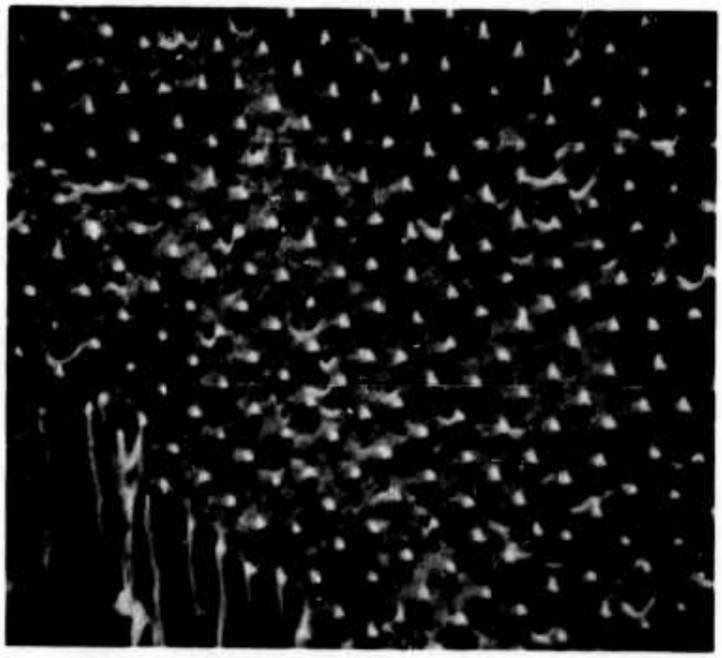

b) X 2950.

Figure 34. Silver Solder Surface Formed After Prying Sandwich Structure Apart. Scanning Electron Micrographs.

procedures (i.e. sample precleaning, atmosphere control, selective vaporization of the Ag, etc.) and, consequently, further testing of additional braze materials was initiated.

B. PLATINUM BRAZING

Platinum brazing was investigated for several reasons. First, it would be advantageous to final etch an emission sample after the electrical and mechanical contact has been established to the cathode structure. This reduces the chance for fiber damage due to sample handling. The inertness of platinum to acids made it a primary choice for a braze, whereas silver solder was suspect to acid attack. Secondly, part of the procedure for silver brazing involved precleaning the sample and support in H_2 at 1100°C. Cleaning added an hour to the process as the furnace had to be cooled to room temperature to introduce the braze into the system and then reheated to the 750°C brazing temperature. Platinum brazing would eliminate an extra precleaning as the melting point of platinum is 1720°C, and H_2 would remove any oxide layer during heating to the brazing temperature. Third, exceeding the brazing temperature of the silver solder caused preferential vaporization of the braze components. The low vapor pressure of platinum would allow a 200 to 300°C brazing range above the melting point.

Platinum brazing does present several disadvantages. Brazing at 1750°C is not amenable to any laboratory. Also, the

cost of platinum is undesirable as brazing 0.2 cm^2 of sample requires $5.00 of platinum. A brazing test with platinum showed two other disadvantages.

A sample of UO_2-W was sandwiched between two molybdenum discs with 4 mil platinum foil between the sample and the discs. Brazing in H_2 at about 1800°C resulted in brazing only part of the UO_2-W sample to the molybdenum disc. Where there was sufficient platinum, brazing appeared to have been successful. However, the platinum wet the molybdenum discs to the extent that platinum almost completely surrounded the bottom Mo disc and half the top disc. SEM micrographs were made of the sample and disc after the discs had been pryed apart. Virtually no wetting of sample surface occurred. In most areas the platinum "balled up" on the surface of the composite, Figure 35. Only in a few small areas, Figure 36, did the braze flow between the pins on the composite. The braze surface revealed mostly platinum crystals, Figure 37, with little or no evidence of pin wetting. In a few small areas, presumably corresponding to the regions where the platinum did flow between the pins, the W pins were embedded in the braze, Figure 38. During brazing, the platinum may have flowed over the molybdenum discs too rapidly and the resultant platinum layer was so thin that satisfactory wetting was only achieved in the isolated areas where adequate contact was evident. Had an increased amount of platinum been used, it is possible that larger areas of good wetting would have been found.

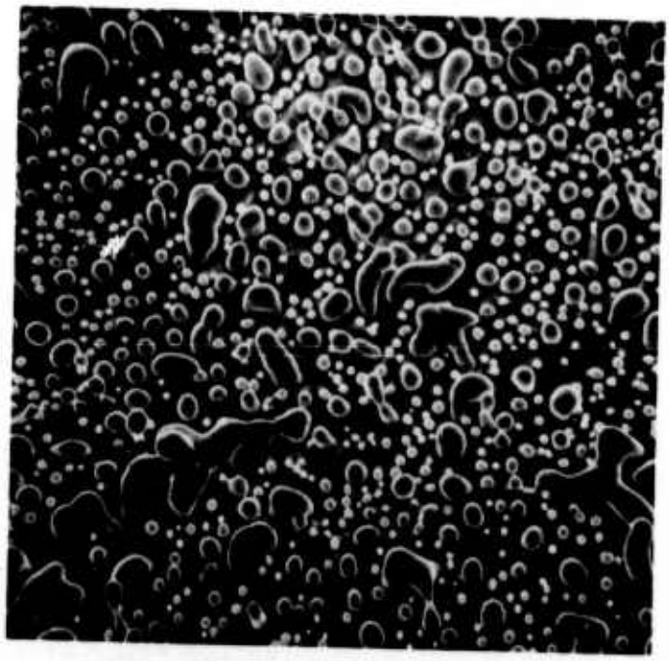

Figure 35. Platinum Globules on UO_2-W Surface After Brazing. Scanning Electron Micrograph, X2,600.

Figure 36. Isolated Area of UO_2-W Surface Where Platinum Wet the Surface and Flowed Between the W Pins. Scanning Electron Micrograph, X6,500.

Figure 37. Surface of Platinum Braze Showing Small Crystals and Absense of Fibers. Scanning Electron Micrograph, X2,400.

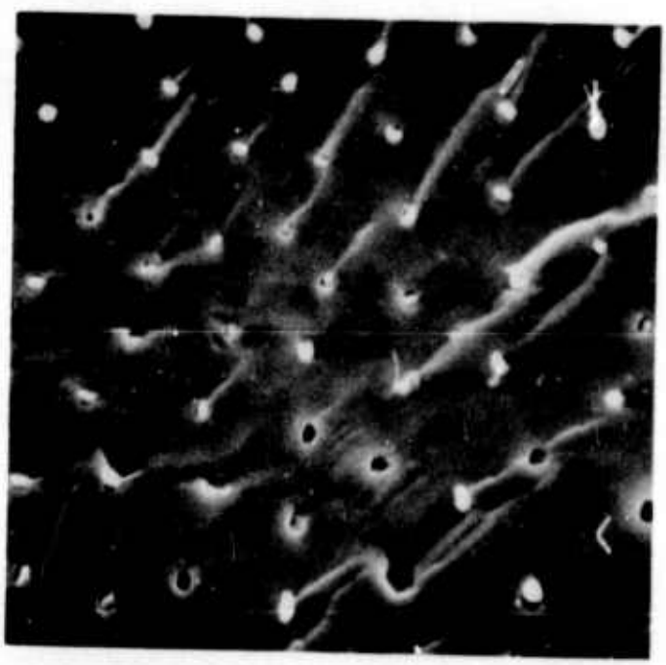

Figure 38. Isolated Area in Platinum Braze Surface Showing W Pins Embedded in the Braze. Scanning Electron Micrograph, X6,000.

C. COPPER BRAZING

Concurrently with the silver-based brazing tests, attempts were made to braze both UO_2-W and Gd_2O_3-Mo composites to molybdenum using pure copper in a hydrogen atmosphere. Brazing was accomplished by coupling to the molybdenum substrate and copper in an rf field, heating until the copper melted at 1080°C, increasing the temperature 50-100°C above the melting temperature, and holding for 10 minutes. The copper appeared to wet and adhere to both the UO_2-W and Gd_2O_3-Mo composites. As in the silver solder brazing, SEM examination of the copper surface after brazing, Figure 39, showed tungsten fibers pulled from the UO_2 matrix and embedded in the copper braze. A polished cross section of a UO_2-W:Cu:Mo sandwich arrangement viewed in reflected light indicated good contact between the copper and the UO_2 matrix.

Vaporization of the copper has not been a problem, and to date a "sound" copper braze has been routinely achieved. The mismatch in thermal expansion of the composites and the molybdenum support has produced some microcracking along the cell boundaries in the composites after brazing (expecially in the UO_2-W samples).

To eliminate this microcracking, metals other than molybdenum were considered for supports. Copper is reactive, however, and a metal with proper thermal expansion characteristics that does not react with the copper has been difficult to find. Work will continue in this area. A less reactive

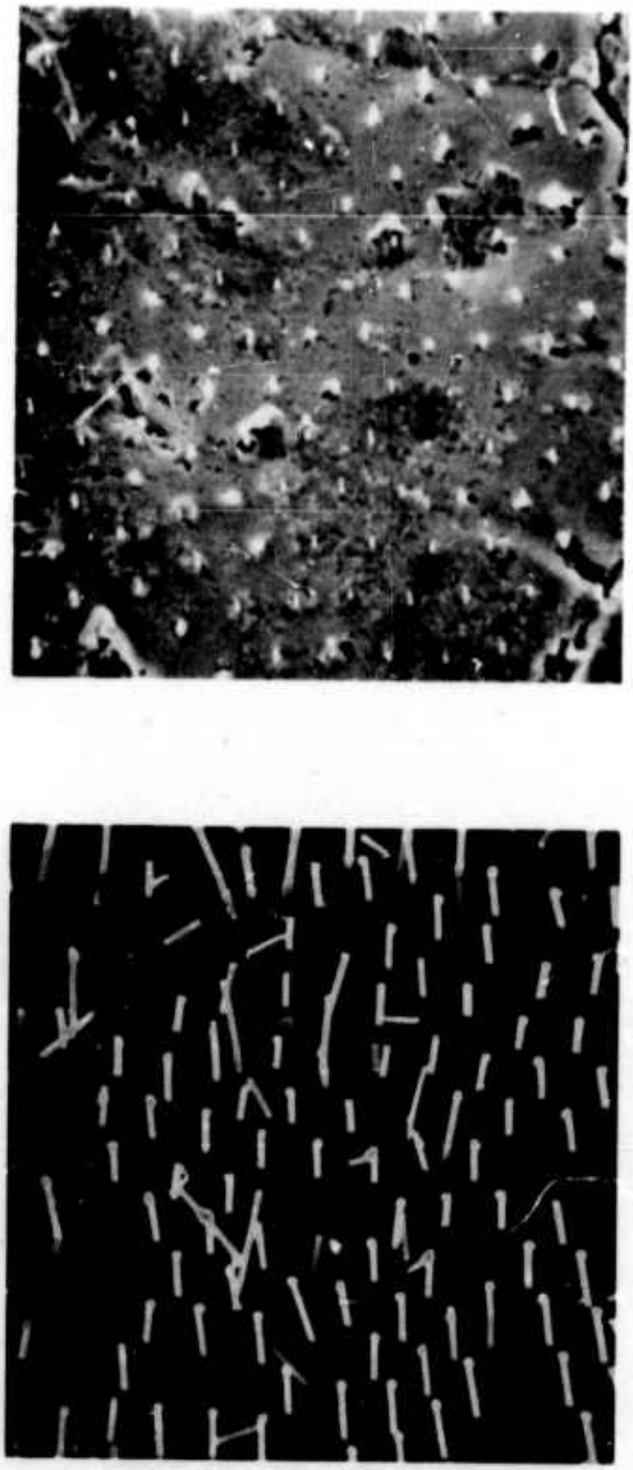

Figure 39. Scanning Electron Micrographs of Two Areas of the Cu Braze Surface Showing W Pins Pulled From the UO_2-W Composite. X2,100.

braze (Handy and Harman's "Permabraze 130") was considered to allow use of supports other than molybdenum. This braze is reputed to wet molybdenum and tungsten well and to be non-reactive, but contains gold and is very expensive.

There is one disadvantage using the copper braze with the UO_2-W samples. The CrO_3-based etching solutions used to form the emitting arrays are ineffective once the composite has been brazed using pure copper. Apparently an electro-chemical potential is generated between the Cu braze and the UO_2-W composite which stops the etching process. Consequently the UO_2-W samples must be etched to form the emitting arrays prior to Cu brazing. The Gd_2O_3-Mo samples are chemically etched in a sulphuric acid-based solution and this etchant works well on the composite, after Cu brazing to a molybdenum support structure. A continuing effort is underway to select brazing materials and conditions which will improve and simplify the braze-etch procedures used to form the emitter structures.

SECTION V

EXPERIMENTAL EMISSION MEASUREMENTS

This section discusses the experimentally observed high field electron emission characteristics of the oxide-metal composite materials. A variety of sample configurations were tested ranging from emitter fibers having long blunt tips to those with pointed tips. During the investigation, a brazing technique supplanted the previously used silver paste as the emitter attachment medium. Apparently as a result of this change, the available current densities increased significantly, until several hundred mA/cm^2 could be routinely obtained. Two different test diode structures were used in the study. The majority of the emission data were DC, but pulsed measurements were initiated.

A description of the experimental apparatus is given, and the most significant of the experimental results are discussed.

A. EXPERIMENTAL APPARATUS

Two different test diode structures were used during this report period. The first of these which allowed the variation of the interelectrode spacing from the outside of the vacuum system has been described previously.[3] While the ability to

vary the interelectrode spacing was desirable, it was found that the device had inadequate heat dissipation and was consequently unstable in high current operation. To remedy this significant defect, the test diode shown in Figure 40 was constructed. As can be seen from the photograph, the diode was constructed from two high current electrical feedthrough insulators with 0.75 inch diameter copper shanks. The molybdenum sample holder and anode were then attached to milled flats on the feedthroughs. Final machine work was done on the assembly in situ so the copper supports are parallel to within 0.001 inch. A 0.375 inch diameter well has been drilled in both of the copper supports. This allows the insertion of 1000 watt cartridge heaters for use during bakeout and also provides a cooling well through which water was circulated when the diode was operated. The heaters allowed baking of the diode assembly to 400°C which was the limit set by the feedthrough construction. During emission testing, the cooling was sufficiently efficient to hold the anode temperature rise to a few degrees; thus, changes in interelectrode spacing due to thermal expansion were effectively eliminated.

The prototype demountable diode is shown in Figure 41. It was constructed from a Conflat-flanged 2-3/4 inch diameter pyrex nipple. The anode and cathode assemblies were attached to the respective end plates with a copper pumping tube exiting at the cathode end. The diode may be pumped through the copper tube and pinched off from the vacuum system once the proper vacuum is achieved. An ion-pumped system in conjunction with

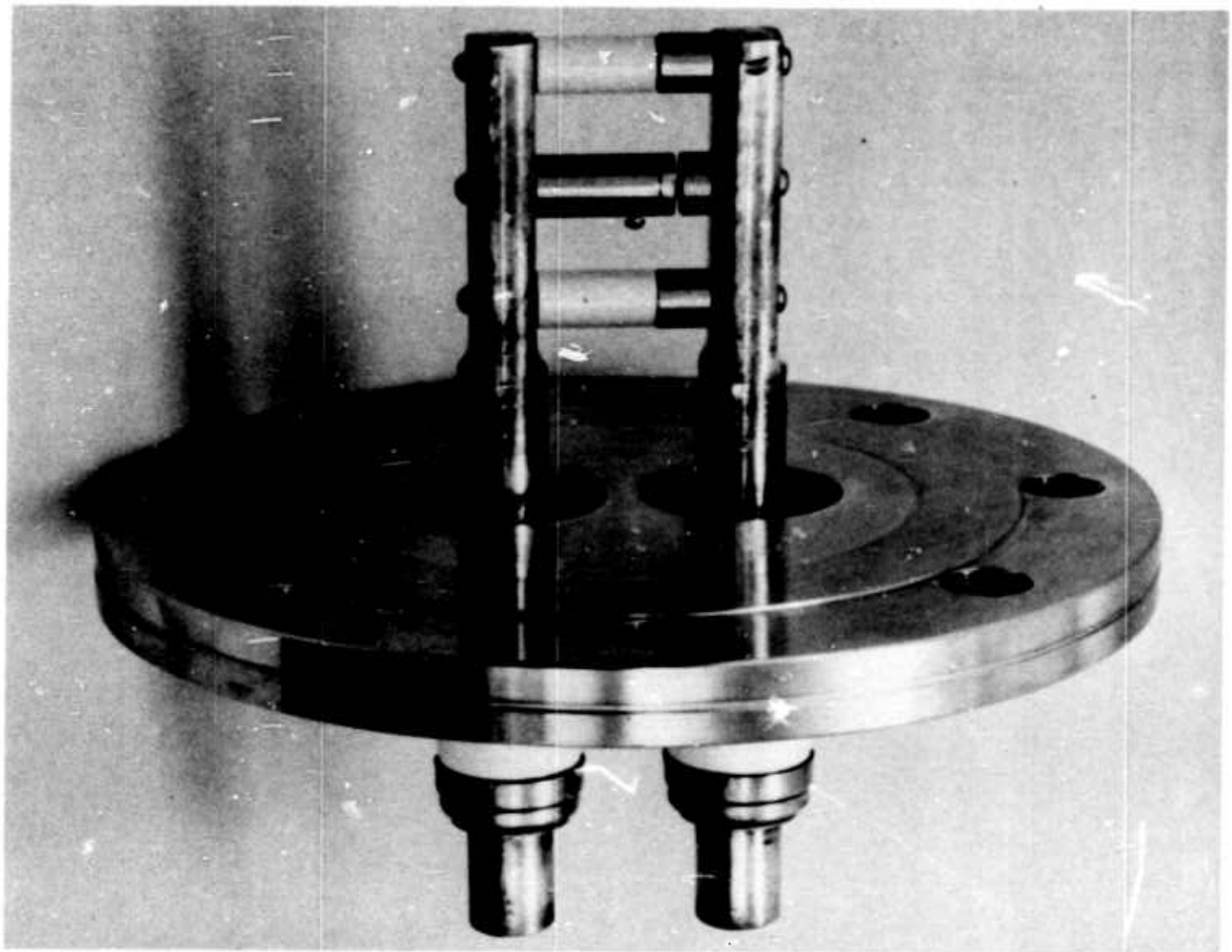

Figure 40. Photograph of Water-Cooled Constant-Spacing Test Diode.

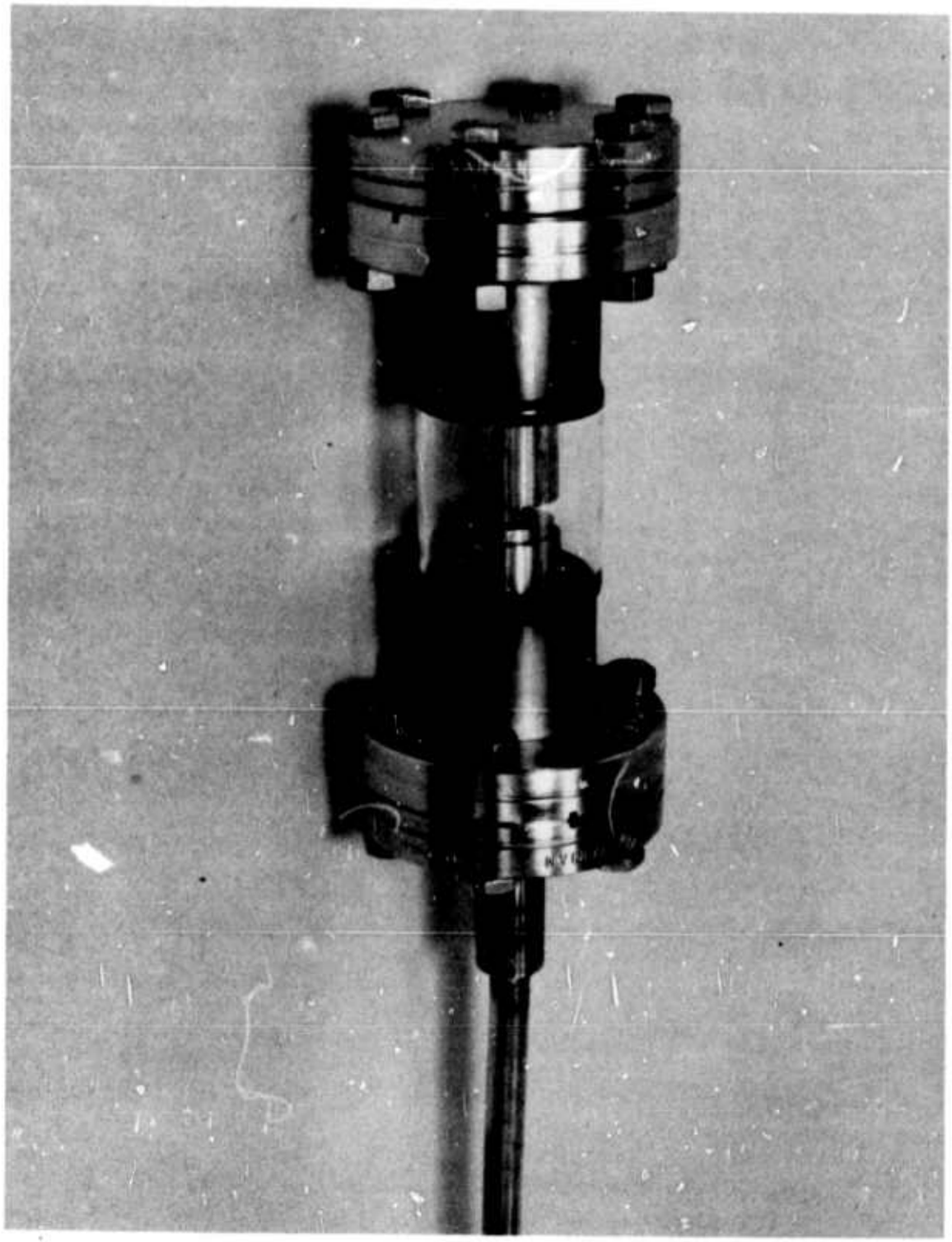

Figure 41. Photograph of Prototype Demountable Test Diode.

a sorbent-type forepump is used with the demountable diode. This diode which is presently undergoing initial tests will be used in a variety of future experiments, to be discribed in subsequent reports.

B. ELECTRON EMISSION MEASUREMENTS

A chronological summary of the emission data together with important emitter characteristics for all samples tested since the last report is given in Table III. Several important milestones of the research are indicated in Table III. On pumpdown No. 36 a brazing technique replaced the silver paste as the medium for attachment of the sample to the cathode assembly. This change was accompanied by a noticeable increase in emission current density. Several Gd_2O_3-Mo samples were tested; these gave fair results, but generally inferior to the UO_2-W type emitter. On pumpdown 37, a UO_2-W sample having pointed pins gave an emission current of 500 mA/cm^2. This experiment was terminated by failure, due to excessive power dissipation, of the variable spacing diode assembly. After one additional pumpdown, the water-cooled constant-spacing diode described above was used. The remaining tests were concerned with increasing the maximum obtainable current density through a variation in emitter morphology and improvements in experimental techniques including preconditioning of the emitter. Preliminary pulsed emission data were also obtained. While the experiments listed in Table III are quite varied in nature, it is helpful if they are discussed with reference to certain

TABLE III

CHRONOLOGICAL SUMMARY OF EMISSION EXPERIMENTS

Installation Date	Pump-Down No.	Sample Designation	Type of Composite	Emitter Configuration	Maximum Current Density ma/cm^2	Active Emitter Area cm^2	Remarks and Notes
29 June 1972	32	13-57/11-39	UO_2-W	Long, stringy fibers	No emission testing	-	Initial testing of residual gas analyzer; analyzer filament burned out.
5 July 1972	33	13-57/11-39a	UO_2-W	Short, blunt fibers	84	0.04	Testing interrupted by power outage, thus requiring another pumpdown for continued testing.
16 July 1972	34	13-57/11-39a	UO_2-W	Short, blunt fibers	90	0.04	Unstable emission.
27 July 1972	35	22-13/11-41b/ 23-5	Gd_2O_3-Mo	Very high fiber density	80	0.079	Arcing occurred when more than 80 mA/cm^2 was produced.
5 Aug 1972	36	13-57/11-39b/ 23-8	UO_2-W	Long, blunt fibers	330	0.061	Composite brazed to Moly cathode.
16 Aug 1972	37	13-57/11-14-18/23-12	UO_2-W	Pin tips pointed by etching	500	0.10	Composite brazed to Moly cathode, testing terminated by short circuit.
31 Aug 1972	38	13-90/11-44/ 23-15/38	UO_2-W	Sharpened pins	300	0.04	Interelectrode spacing fixed by Al_2O_3 cylinder.
29 Sept 1972	39	22-34/39,40	Gd_2O_3-Mo	Short, blunt fibers	-	0.045	Used constant-temperature fixed-spacing diode. Cathode shorted to ground.

TABLE III (Continued)

Installation Date	Pump-Down No.	Sample Designation	Type of Composite	Emitter Configuration	Maximum Current Density mA/cm^2	Active Emitter Area cm^2	Remarks and Notes
8 Oct 1972	40	22-34/39,40	Gd_2O_3-Mo	Short, blunt fibers	440	0.045	Constant-temperature fixed-spacing diode used on this and subsequent pumpdowns.
14 Oct 1972	41	113-6/41	UO_2-W	Sharpened pins	600	0.034	600 mA/cm^2 lasted only a few minutes; emission density of 150 mA/cm^2 for about 130 hours.
28 Oct 1972	42	113-6/113-12	UO_2-W	Several sharp pin areas destroyed by re-etching	200	0.034	Re-etched sample of pumpdown number 41.
8 Nov 1972	43	27-5/113-15/43	UO_2-W	Sharp pins; several cracks in UO_2 matrix	-	0.317	Portions of the cracked matrix lodged between anode and cathode, terminating test sequence.
16 Nov 1972	44	13-57/11-51/44	UO_2-W	Sharp pins	50	0.04	Poor emission
23 Nov 1972	45	25-32/11-52/45	UO_2-W	Sharp pins	400	0.10	Used high value of series resistance; arcs occurred at 600 mA/cm^2.
6 Dec 1972	46	22-47/46	Gd_2O_3-Mo	Blunt pins	-	0.05	Vacuum system failure destroyed the sample before significant data were obtained.

common attributes. On such a basis the following categories evolved: (1) the effects of emitter pin shape on emission; (2) possible effects of pre-conditioning on emission and emitter lifespan; and, (3) results of pulsed-mode experiments.

1. Effects of Emitter-Pin Shape on Emission

An analysis of the data in Table III reveals that the largest and most stable emission currents were observed with samples which had either very long fibers ($>10\mu$) or short fibers having sharpened tips. This behavior can be tentatively explained by an examination of the effective (enhanced) electric field present at the emitter tips.

High and stable electron emission is obtained when a large fraction of the total pins participate in the emission process. This can occur when: (1) the emitter tips are all identical and thus have the same enhancement factor; (2) when pin size and length are such as to make the local electric field independent of tip radii variations; or(3) when some dynamic mechanism acts to alter the pin-tip shape in a manner tending to produce a more uniform array.

The eutectic growth process used to form the oxide-metal samples inherently can never produce an array of perfectly uniform pins, so high and stable emission occurs only when one of the two other equalization mechanisms is active. A recently derived approximation[7] indicates that the field enhancement factor approaches a saturation value for 0.3μdia. pins having a length of 20μ. The enhancement factor is essentially independent,

to within about 20 percent, for pin radius changes of an order of magnitude about the nominal value. This is to be contrasted with the order of magnitude change in enhancement factor when the radius of 2μ high pins is varied a like amount. Therefore, stable emission cannot be achieved with short pins of initially nonuniform radii unless there exists some other mechanism for dynamically producing uniform radii. The present experimental work indicates that a dynamic improvement in current sharing was possible when finely sharpened emitter pins were employed in conjunction with the process outlined below.

Consider an array of sharpened pins whose radii are distributed about some nominal value. If an increasing macroscopic electric field is applied to the array, those pins having the sharpest tip radii and hence greatest microscopic electric field will be the first to emit significant numbers of electrons. As the field increases, the perhaps one percent of the pins with the sharpest tips will produce almost all of the macroscopic current. These favored pins may, due to joule heating, reach a local temperature at which significant surface migration and localized melting will tend to round the tip, thus increasing the radius. This will lead to a decrease in current emitted by the favored pins and allow the entire ensemble of pins to develop a higher total current, whenever the macroscopic electric field is further increased. Note that the shaping process produces an initial decrease in current, but subsequently permits a higher total current without pin

damage when a larger fraction of the total number of pins is activated. However, if the pins are subjected to a too rapidly increasing electric field, the smoothing process may not proceed fast enough to prevent excessive heating of some pins and accompanying destruction by vacuum arcs.

The effects discussed above can be illustrated by a study of experimental data typical of the blunt and sharpened pins. Figure 42 shows a scanning electron micrograph of Sample No. 13-57/11-39b/23-8, Pumpdown No. 36, which as can be seen had long fibers. A field emission electron current density of 330 mA/cm^2 was obtained from this sample. It should also be noted that Sample No. 11-57/11-31c, the best discussed previously[1], also had this morphology.

Sample No. 13-57/11-14-18/23-12/37 which gave a current density of 500 mA/cm^2 provides an interesting illustration of pin-tip blunting. Figure 43a shows the emitter before operation in the test diode; note that the pin-tips are quite sharp. Figure 43b shows a scanning electron micrograph of the same sample after operation at the 500 mA/cm^2 current density. The pin-tips show an obvious onset of rounding. This particular emitter gave its high value of emission current while sustaining little overall damage. Since selective rounding of the pin tips apparently produced a more stable emitter, it is important to examine exactly how this process can be realized. This is discussed in the following section.

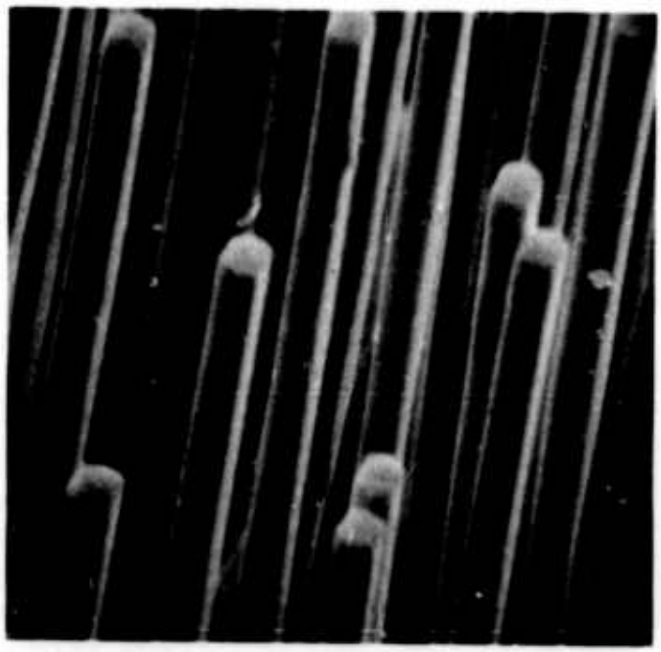

Figure 42. Scanning Electron Micrograph of UO_2-W Sample No. 11-57/11-39b/23-8 Showing Long But Blunt Pins. X12,700.

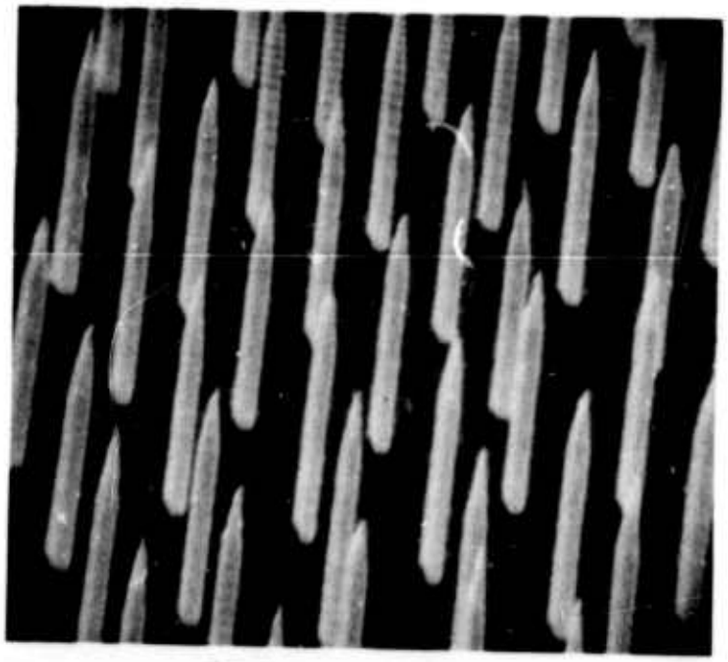

a) Pre-Emission Micrograph Showing Very Sharp Pin Tips. X6,200.

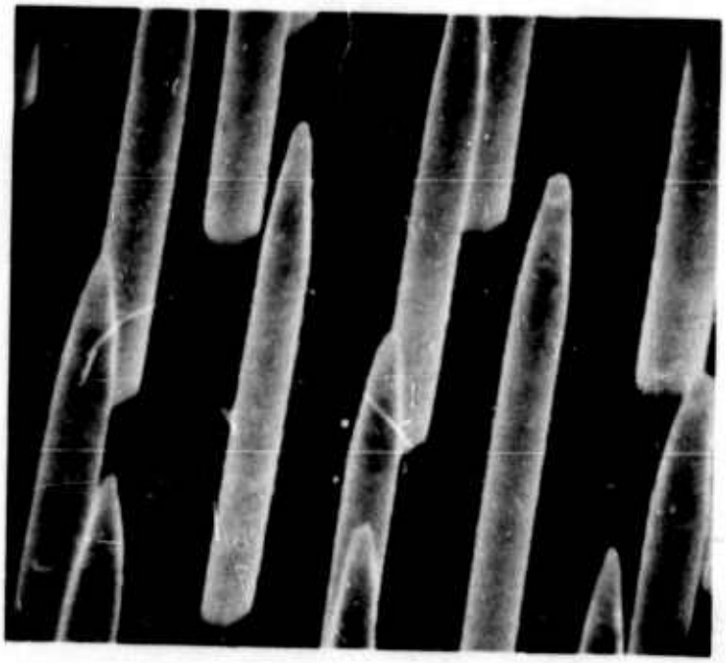

b) Post-Emission Micrograph Showing Blunted Pin Tips. X11,700.

Figure 43. Scanning Electron Micrographs of UO_2-W Sample No. 13-57/11-14-18/23-12/37.

2. Effects of Pre-Conditioning on the Emitters

It has long been recognized that a period of "conditioning" is necessary if a spark gap is to withstand maximum potential.[8] This effect is associated with a blunting of microscopic protrusions on the gap electrodes which initiate the breakdown via high field emission. In the present situation the same process can be used to selectively blunt those emitter tips having the sharper points, thus bringing them closer in radii to the average pin. This process can be accomplished if the maximum emitted current is slowly increased as the pin-tips become desharpened. If the maximum current is allowed to increase too rapidly, those pins with the sharper radii will be destroyed.

Experimental data indicates that conditioning can result in an improvement in maximum current and lifetime of the oxide-metal composite emitters. This conclusion was reached when the behavior of emitters operated with and without a large series resistance was noted. Most early emission tests were made with a high value of resistance (10^6 ohms) in series with the diode. This was done to preclude "dumping" the charged power supply filter capacitors into the sample should a breakdown occur. To reduce the voltage drop and allow higher values of emission current, this resistance was later reduced in value to 50 k-ohms. It was suspected and later confirmed by careful observation that samples tested with the smaller series resistance were likely to give a large value of initial

current but the value subsequently decreased one or two orders of magnitude over a few hours time interval. With the high resistance in the circuit, the initial current was not as large, but tended to increase with time. It was then observed that if a large resistance was used initially and the emitter operated for a period of a few days with gradually increasing current, a smaller resistance could be inserted, the current further increased, and little decay would occur. From these observations it is tentatively concluded that the initial operation in a current-limited-mode probably tends to equalize the individual pin-currents by blunting and thus permits a larger gross current without damage occurring to the spikes. The validity of this conditioning procedure is now undergoing additional study.

An example of how alterations in emitter geometry caused by pin destruction effects the emission is seen in Figure 44. The figure shows three consecutive Fowler-Nordheim plots taken for Sample No. 113-6/41 over a period of two days. The first two plots were taken about four hours apart on the first day, while the third was taken about 24 hours later. They illustrate the progressive deterioration of an emitter which was operated initially with a low value of series resistance. No conditioning process was used on the emitter.

3. Pulsed-Mode Emission Measurements

Preliminary pulsed-mode high field emission data have been obtained for a UO_2-W type emitter. A pulse of variable

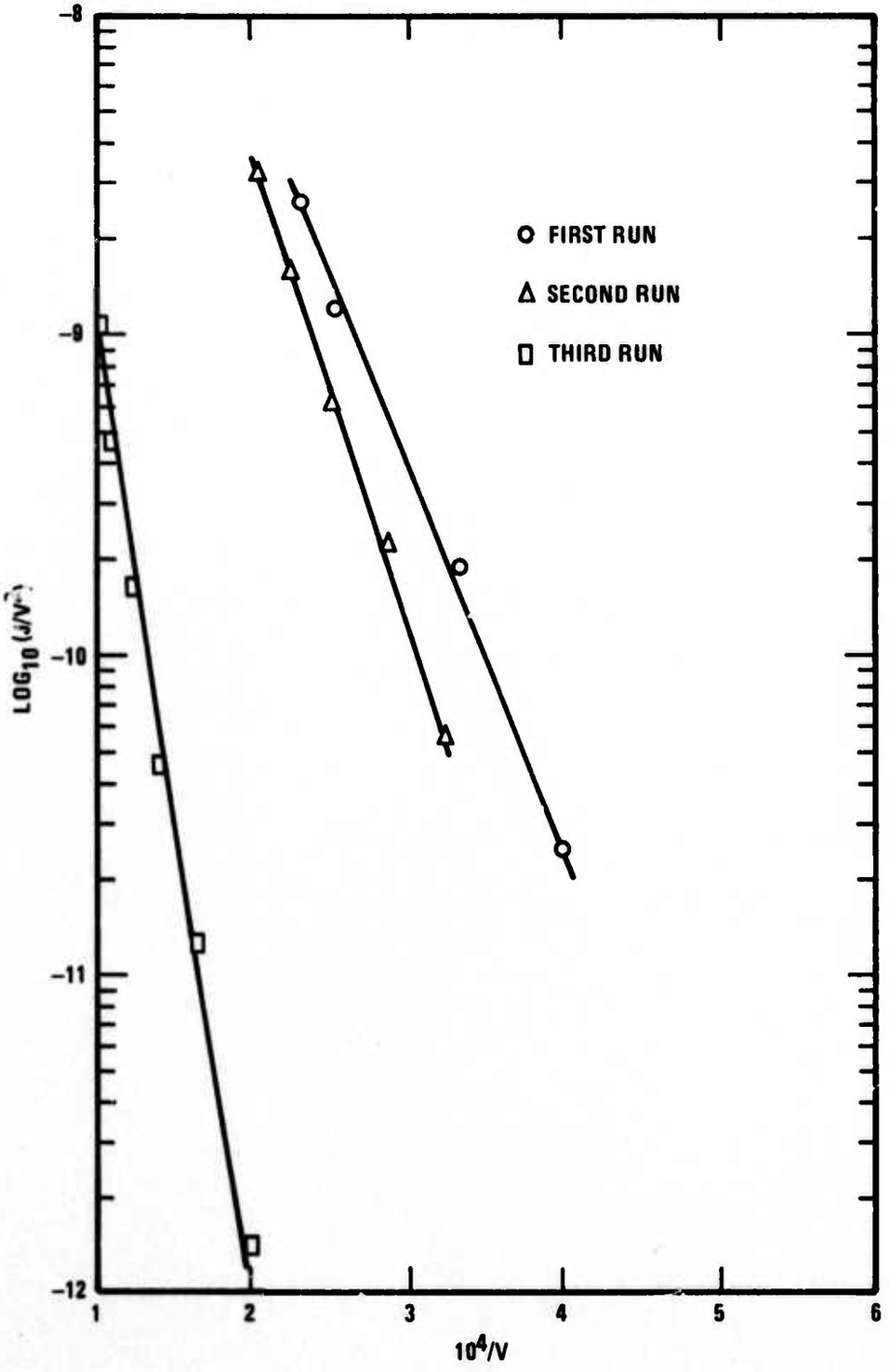

Figure 44. Fowler-Nordheim Plots for UO_2-W Sample No. 113-6/41, J in A/cm^2 and V in Volts.

length from 10 to 500 microseconds was used in the experiment. The pulse was obtained from a hard-tube type pulse amplifier using a 4-X-150 tube. Because the maximum output voltage of the pulse amplifier was only about 3 kV, a clamping circuit was employed to offset the pulse by 0 - 6 kV above ground. Since the high field emission current is exponentially sensitive to the applied voltage, more than 95 percent of the total current was produced by the 3kV pulse portion of the total potential. Some problems were encountered with circuitry due to the long lead lengths used in the initial setup. An oscilloscope trace of some preliminary data is shown in Figure 45. The overshoot on the rising and falling portions of the current trace is due to the diode capacitance. For the same voltage, the peak pulsed current values were the same as those measured under dc conditions. Since the average power dissipation is directly related to the duty factor, it is likely that considerably greater peak currents can be obtained in the pulsed mode. Additional measurements, with pulse generators of higher power, will be required to confirm this speculation.

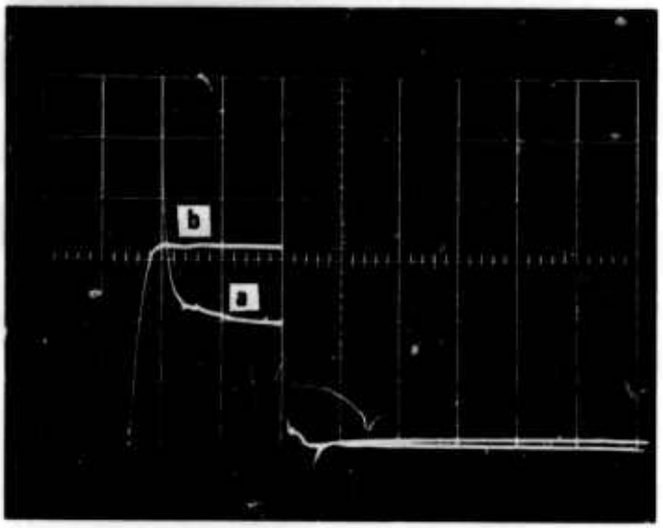

a) Emission Current, 0.4 ma/div.

b) Applied Voltage, 1 KV/div., Base Line 4 KV,

Time Scale 20 μs/div., Duty Factor 5×10^{-4}.

Figure 45. Oscilloscope Trace of Pulsed-Mode Electron Emission from UO_2-W Composite.

SECTION VI

THEORETICAL ANALYSIS OF ELECTRON EMITTING ARRAYS

A. INTRODUCTION

In an earlier study[9], the calculation of the electrostatic potential distribution surrounding a square array of charged surface states on an insulating dielectric substrate was presented. The potential was determined by imaging the surface states through a grounded conducting planar anode and by solving the appropriate Poisson equation by using a harmonic mode expansion of the potential distribution in each cell, which consisted of a surface state and its image. The resulting undetermined coefficients in the series expansion were computed by applying the Neumann boundary conditions at every common cell interface. The resulting form of the solution for the potential distribution was a double Fourier series.

In a later study[2], the surface charge states were replaced with the finite conducting pins of the actual device, which protrude out of the insulating dielectric substrate. Therefore, an attempt was made to generalize the earlier model to include the more important parameters of the pins themselves, e.g. pin shapes, pin heights, and pin cross-sectional areas, which were not present in the earlier model. This generalization of the earlier model, of course, severely complicated the problem and necessitated the use of several approximations in order

obtain a solution in a useable form. Several mathematical models were developed to calculate the potential distribution in the neighborhood of the conducting pins. An actual three-dimensional solution was not obtained; instead, two orthogonal cross-sectional cuts of the device were analyzed. In each case, the appropriate Laplace equation was separated in a rectangular coordinate system. Each resulting separated equation was then solved by using a harmonic mode expansion. The resulting undetermined coefficients in the recombined product series expansion were computed by applying the continuity conditions on the potential and its first derivative at all common interfaces. The resulting form of the solution for the potential distribution was a double Fourier series.

In the present study, a purely numerical approach is being considered. It was observed in the previous studies that the analysis was complicated by the periodicity of the structure and by the closeness of the planar anode structure above the pins. The solution to the Laplace equation for a device with non-periodic spacings of the pins, or with pins of a geometry for which the Laplace equation is inseparable, is very complicated if not impossible to solve, and at best will produce a solution in the form of a slowly converging infinite series. An alternate approach to this problem is to solve the Laplace equation by a purely numerical-type solution and to implement this solution on a high speed computer.

B. NUMERICAL SOLUTION

A numerical program has been developed to solve Laplace's equation numerically in a cubical region of space[1]. The cubical region of space may contain various subregions containing conducting material, but may not contain any subregions containing free charge or current. The exterior surface of the cube may or may not have fixed boudary conditions specified on it, i.e. if fixed Direchlet boundary conditions are not specified, then Neumann boudary conditions are assumed.

The program was tested to determine the validity of the numerical algorithm, and good convergence, with an error of less than one percent, was obtained in approximately 30 seconds of actual central processing time. The geometry of the test case was one for which the exact solution could be determined apriori by analytical means, via that of a hollow conducting cube with five sides grounded and with one side floating at a fixed potential specified as any one of the countable infinity of non-summed rectangular eigenfunctions for the cube. For simplicity, the $x = 1$, $y = 1$ mode was chosen.

This program, however, was limited to the available core space in the memory of the UNIVAC 1108 computer. In order to use this program for multiple pin geometries, as found in an actual emitter, a larger core space was required to approximate the curvature of the continuous pin surfaces with a discrete cubical grid, so that exact derivatives in the field

intensity calculations could be obtained. Therefore, it was necessary to enlarge the core space available to the program. This necessitated the use of a virtual memory device such as a high speed drum and a system routine such as NTRAN. There were four devices which would serve this purpose, ranging from a high speed, low storage drum to a low speed, high storage drum. Unfortunately, the highest speed drum was too small to handle the large core requirements needed, and the next fastest drum was selected. The virtual memory of this device, presented large input/output times to the program due to the overhead of several check routines associated with the transfer error tests on every read or write command. The total run time was on the order of 30 minutes. The actual central processing time, however, was not too large. The total CPU time was on the order of 30 seconds. Due to the complexity of the EXEC 8 processor, however, it seldom completed the entire execution of the program without some type of system error which destroyed part or all of the intermediate computations stored in the virtual memory. Therefore, a different approach was undertaken.

The three-dimensional volume of interest was subdivided into numerous cubical subgrids. Then, each subgrid, in turn, as called by the program logic, was transferred in or out of virtual memory as a complete unit. The subgrid size was chosen as large as could be held in the active memory of the computer. Since the subgrid sizes were large, the number of transfers

were small, and the input/output time was drastically reduced over the earlier attempts. In order to implement these changes, the logic of the program had to be entirely changed. The program was modified to extrapolate potential values to each surface of each subgrid to store separately both the interior volume and exterior surfaces of each subgrid, and to iterate until each common subgrid surface converged to the same potential values on each side of each subgrid. The revised program, unfortunately, then became too complex to compile on the FORTRAN compiler. It was discovered that on the third pass of the compiler through the program on its backward sweep (phase 3), the FORTRAN optimizer routine runs out of table space for the repeated dummy variables. This table space requirement was overcome by segmenting the program into six separate files: viz. main control, sequencing, potentials, fields, currents, and plots. Each segment was then stored on the slowest but largest FASTRAN drum under different file and element names. Even then, several elements routines (sub-routines and sub-functions) failed to produce a relocatable element during computation, but it was later found that these elements could be inserted onto the FASTRAN drum in a demand mode from a remote terminal. After the entire symbolic program on the FASTRAN drum was compiled and all relocatable elements were formed, the program could be mapped into an absolute element file and executed.

One problem still remained, in that the number of drum unit names was also limited by an internal table in the EXEC 8

processor. It was later found that an executive request system routine, ERTRAN, could be called which would swap drum files during actual run time. This routine was used to pair the allowable drum units with the unallowable drum files.

A listing of the programs along with a sample run of a single pin centered under a conducting anode is available. The programs are rather extensive and consequently are not listed in this Report. They are, however, available to any interested individual on request.

SECTION VII

SUMMARY

During the last two and one-half years, oxide-metal composite structures suitable for electron emission testing have been melt-grown under ARPA Order No. 1637. The primary objectives of this study are to understand the growth process and parameters leading to ordered composite structures during controlled solidification of various oxide-metal mixtures and to produce samples suitable for property evaluation. To meet these objectives the research program is divided into five areas: 1) Solidification Behavior of Oxide-Metal Mixtures, 2) The Formation of Optimum Emitting Arrays, 3) Oxide-Metal Composite Properties, 4) Experimental Emission Measurements, 5)Theoretical Analysis of Electron Emitting Arrays.

During the current report period, extensive solidification studies continued in the systems CeO_2 doped Gd_2O_3-Mo and UO_2-W. The initial melting of CeO_2-Mo mixtures is reported. A limited amount of additional information is also presented for the systems Y_2O_3 stabilized ZrO_2-W and HfO_2-W. In the stabilized ZrO_2-W system, it was noted that the growth atmosphere controls the W solubility. Analysis of SEM micrographs of Y_2O_3 stabilized HfO_2-W samples were used to estimate a eutectic composition of approximately 2.5 w/o W in this system.

In the UO_2-W system, the analysis of the influence of stoichiometry changes in the molten oxide on W solubility continued. Many composite growth experiments were run in various CO-CO_2 ratios in an effort to increase the oxygen potential of the growth atmosphere above that available in previous N_2-H_2 gas mixtures, and maintain the O/U ratio in the molten oxide above 2.00. Since this approach provided only limited improvements in the oxide-metal structures, the CO-CO_2 atmospheres were combined with additional changes in the UO_2-W growth procedures designed to achieve "steady state" conditions during solidification. In this procedure essentially all of the interior of a rod-shaped sample was maintained molten, in a fixed CO-CO_2 atmosphere, to achieve uniform W solubility throughout the melt. These modifications produced several centimeters of well ordered UO_2-W composite structures and indicated, based on limited information, that the quantity of W in solution can be varied between about 1.5 to 3 w/o W, depending on the oxygen pressure in the growth atmosphere. This variation in W content also caused changes in pin spacing, at equivalent lowering rates, and consequently provides another useful parameter in controlling the geometry of the electron emitting arrays.

In the system CeO_2 doped Gd_2O_3-Mo, the influence of growth rate on fiber density and diameter have been determined; and some general trends of the effect of growth rate on cell morphology and size, and the ratio of platelets to fibers has

been established. Isostatic pressing techniques have been used to provide long rods of uniform density from which composite samples large enough for mechanical measurements have been machined.

The initial growth of CeO_2-Mo samples was achieved this report period. Work in this system is just getting underway and potentially may prove most attractive because the CeO_2-metal eutectic temperatures are significantly below that found in other oxide-metal systems; consequently, CeO_2 may be useful as the oxide matrix for a variety of the lower melting metals.

Several techniques were used to inductively melt Al_2O_3 and Al_2O_3-Cr_2O_3 mixtures with W and Mo. It was difficult to achieve and maintain molten zones in these materials, and examination of the solidified regions indicated little if any metal solubility in these oxides.

Analysis of the eutectic composition in several of the oxide-metal systems was used to obtain equations describing an apparent change in eutectic composition with growth rate. Surprisingly, but unexplained at present, several of the systems show a minimum in their eutectic composition at intermediate growth rates. Chemical or mechanical parameters are under consideration as causes for this behavior.

A considerable effort was devoted to reworking portions of the electron beam furnace to adapt it to melt and solidify oxide-metal mixtures contained in refractory metal crucibles. A $MgO \cdot Al_2O_3$-Mo mixture was successfully melted using this

equipment; however, there was no indication of tungsten solubility in this compound.

This initial x-ray analysis of several rare earth oxide-Mo composites are reported. Comparative analysis of diffraction patterns from the CeO_2 doped Gd_2O_3-Mo samples indicated that in the "as-grown" condition the oxide matrix contained a sizable amount of mechanical strain which can be relieved by simply grinding the samples.

An extensive investigation of the effect of different etchant compositions and temperatures on the etching characteristics of the UO_2-W samples was performed. Based on this work a set of etching conditions and procedures were established which could routinely form undamaged pointed W pins extending above a smooth UO_2 matrix. In addition, an interesting geometry was discovered in this work where pointed W pins were recessed in holes in the UO_2 matrix. This geometry is potentially interesting for forming arrays of low voltage "electron guns". The initial etching of CeO_2 doped Gd_2O_3-Mo samples is reported, and etchants based on sulphuric acid have proved useful to expose and point the Mo fibers in samples from this system.

Little work was accomplished this report period measuring the basic composite properties because a major effort was expended developing suitable brazes to make both an electical contact and mechanical bond between the composites and metal support structures. A variety of braze materials were tested,

and pure copper turned out to work best between both UO_2-W and Gd_2O_3-Mo samples brazed to Mo pins or discs. The improved electrical contact with copper was partly responsible for the enhanced emission performance achieved this report period.

The most noteworthy project achievements were obtained from the experimental emission measurements. A variety of emitter configurations were tested. Using a combination of proven brazing, growth and etching conditions, several hundred mA/cm^2 could be routinely obtained from most samples. One sample exhibited greater than 0.5 A/cm^2 for several hours until diode failure terminated the experiment. Examination of this sample showed no gross pin damage but only some pin tip blunting. Such blunting may be a mechanism which can dynamically improve the current sharing characteristics of the emitter arrays. Based on this experimental emission testing, an analysis of the existing emission characteristics and behavior of the oxide-metal composites is presented. Thoughts concerning the conditioning of the samples during the initial emission testing are presented and mechanisms for initiating vacuum arcs, which produces extensive emitter damage, are proposed. Two new diode assemblies were constructed to increase the emission testing capability. Initial pulsed measurements are reported.

The first step in the theoretical determination of the high-field emission current from an electron emitting array is the calculation of the electrostatic potential in the

interelectrode space. In the present study, the case of a single spheroidal pin was considered since the exact analytical solution for this geometry can be determined and, therefore, can be used as a check on the convergence of the numerical solutions. The exact solution of this problem was compared with a three-dimensional numerical approximation of the problem and, good agreement was obtained.

Additional numerical methods were employed to calculate the electric field intensity at the surface of a single emitter pin and to integrate the quantum mechanical expression to obtain the electron current. The complete calculation was also made for the above case. Because of the extensive nature of this calculation, excessive computer time is required to exchange information between the active core of the computer and the peripheral memory devices. Techniques are currently under development to overcome this problem. Presently, the emission current expected from pin arrays of limited geometries can be calculated.

REFERENCES

1. A. T. Chapman, et. al., "Melt-Grown Oxide-Metal Composites", Annual Technical Report (No. 4), ARPA Order No. 1637 and Contract DAAHO1-71-C-1046, School of Ceramic Engineering, Georgia Institute of Technology, July 1972.

2. A. T. Chapman, et. al., "Melt-Grown Oxide-Metal Composites", Semi-Annual Technical Report (No. 3), ARPA Order No. 1637 and Contract DAAHO1-71-C-1046, School of Ceramic Engineering, Georgia Institute of Technology, January 1972.

3. A. T. Chapman, et. al., "Melt-Grown Oxide-Metal Composites", Final Technical Report (No. 2), ARPA Order No. 1637 and Contract DAAHO1-70-C-1157, School of Ceramic Engineering, Georgia Institute of Technology, July 1971.

4. A. T. Chapman, et. al., "Melt-Grown Oxide-Metal Composites", Semi-Annual Technical Report (No. 1), ARPA Order No. 1637 and Contract DAAHO1-70-C-1157, School of Ceramic Engineering, Georgia Institute of Technology, January 1971.

5. L. M. Brown and K. S. Mazdiyasni, "Characterization of Alkoxy-Derived Yttria-Stabilized Hafnia," J. Amer. Cer. Soc. (53) 11 593 (1970).

6. P. Duwez, "The Zirconia-Yttria System", J. Electrochem. Soc. 98 No. 9, 356-362 (1951).

7. H.Pfleiderer and H. Rehme, "Spike Cathode for Field Emission" Phys. Stat. Sol. (a) 11, 153-60 (1972).

8. A. Watson, A. S. Denholm and M. J. Mulcahy, Proceedings-Second International Symposium-Insulation of High Voltages in Vacuum, M.I.T. 1966 (pp. 103-9).

9. J. D. Levine, "The 3-D Electrostatic Potential Surrounding a Square Array of Surface Charges", Surface Sci. 10 313-326 (1968).